MANAGEMENT OF THERMAL RUNWAY IN BATTERIES USING PHASE CHANGE MATERIAL

THESIS SUBMITTED IN PARTIAL FULFILMENTS OF THE REQUIREMENT FOR THE DEGREE OF MASTER OF ENGINEERING IN AUTOMOBILE ENGINEERING UNDER FACULTY OF ENGINEERING AND TECHNOLOGY

Submitted by

SIDDHARTHA BANERJEE

Class Roll Number: 002011204017

Registration Number: 154350 of 2020-21

Examination Roll Number: M4AUT22017

Academic Session: 2020-2022

Under the guidance of

Prof. Achintya Mukhopadhyay

&

Prof. Sourav Sarkar

Department of Mechanical Engineering

Jadavpur University

188, Raja S.C. Mullick Road, Kolkata - 700032

DECLARATION OF ORIGINALITY AND COMPLIANCE OF ACADEMIC ETHICS

I hereby declare that the thesis entitled "**MANAGEMENT OF THERMAL RUNWAY IN BATTERIES USING PHASE CHANGE MATERIAL**" contains literature survey and original research work by the undersigned candidate, as a part of his *MASTER OF ENGINEERING IN AUTOMOBILE ENGINEERING under the DEPARTMENT OF MECHANICAL ENGINNERING*, studies during academic session 2020-2022.

All information in this document have been obtained and presented in accordance with the academic rules and ethical conduct.

I also declare that, as required by these rules of conduct, I have fully cited and referenced all the material and results that are not original to this work.

Name: **SIDDHARTHA BANERJEE**

Class Roll Number: **002011204017**

University Registration No: **154350 of 2020-21**

Examination Roll No: **M4AUT22017**

Date:

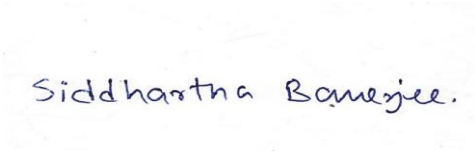

Signature of Candidate

FACULTY OF ENGINEERING & TECHNOLOGY

DEPARTMENT OF MECHANICAL ENGINEERING

JADAVPUR UNIVERSITY

KOLKATA

CERTIFICATE OF RECOMMENDATION

This is to certify that the thesis entitled "**MANAGEMENT OF THERMAL RUNWAY IN BATTERIES USING PHASE CHANGE MATERIAL**" is a bonafide work carried out by SIDDHARTHA BANERJEE under our supervision and guidance in partial fulfilment of the requirements for awarding the degree of Master of Engineering in Automobile Engineering under Department of Mechanical Engineering, Jadavpur University during the academic session 2020-2022.

THESIS SUPERVISOR
Prof. Achintya Mukhopadhyay
Department of Mechanical Engineering
Jadavpur University, Kolkata

THESIS SUPERVISOR
Prof. Sourav Sarkar
Department of Mechanical Engineering
Jadavpur University, Kolkata

Prof. Chandan Mazumdar
Dean
Faculty of Engineering and Technology
Jadavpur University, Kolkata

Prof. Amit Karmakar
Head of the department
Department of Mechanical Engineering
Jadavpur University, Kolkata

FACULTY OF ENGINEERING & TECHNOLOGY

DEPARTMENT OF MECHANICAL ENGINEERING

JADAVPUR UNIVERSITY

KOLKATA

CERTIFICATE OF APPROVAL

The foregoing thesis, entitled "**MANAGEMENT OF THERMAL RUNWAY IN BATTERIES USING PHASE CHANGE MATERIAL**" is hereby approved as a creditable study in the area of Automobile Engineering carried out and presented by SIDDHARTHA BANERJEE in a satisfactory manner to warrant its acceptance as a prerequisite to the degree for which it has been submitted. It is notified to be understood that by this approval, the undersigned do not necessarily endorse or approve any statement made, opinion expressed and conclusion drawn therein but approve the thesis only for the purpose for which it has been submitted.

Committee of final evaluation of thesis:

_____

_____

_____

ACKNOWLEDGEMENT

I am very thankful to my respected thesis supervisor **Prof. Achintya Mukhopadhyay** Sir, Professor, Department of Mechanical Engineering, Jadavpur University and supervisor **Prof. Sourav Sarkar**, Assistant Professor, Department of Mechanical Engineering, Jadavpur University for their excellent and resourceful guidance, which helped me a lot in the completion of this thesis. Without their supervision and constant encouragement it would not be possible to prepare such a thesis compactly. I do convey my best regards and gratitude to them.

The regular discussions and idea-sharing with my thesis supervisors really helped me to improve my knowledge day by day in my research related problems. They were always available for me for any query, whether it was a telephonic or a face to face discussion. Their appreciation and encouragement in this project work really helped me to realize my aspirations towards research work. They were the key persons in my project work and their guidance, supervision as well as providing necessary information in completing my master's thesis is immense.

I am highly indebted to all my professors, their guidance and supervision as well as for providing necessary information regarding thesis and also for their support in completing my master's thesis.

I would like to thank **Mr Saumendra Nath Mishra**, **Mr Anjan Nandi** and **Mr Sudipta Saha** PhD scholars, for giving me valuable suggestions and allowing me to access their systems whenever needed.

I would like to express my gratitude towards my parents and my younger brother for their kind cooperation and encouragement which helped me in the completion of my master's thesis.

Finally, my thanks and appreciations also go to my dear friends in developing my master's project and people who have willingly helped me out with their abilities.

SIDDHARTHA BANERJEE

M.E ("Automobile Engineering")

2nd Year, Final Semester

Department of Mechanical Engineering

Jadavpur University, Kolkata

TABLE OF CONTENTS

3. Numerical modelling

Nomenclature

LIB	Lithium-Ion battery
BTMS	Battery Thermal Management System
TR	Thermal Runaway
EV	Electric Vehicles
PCM	Phase Change Material
Li	Lithium
IC	Internal combustion
1-D	One dimensional
2-D	Two Dimensional
3-D	Three Dimensional
$LiCoO_2$	Lithium Cobalt Oxide
CoO_2	Cobalt Oxide
SEI	Solid Electrolyte Interface
CFD	Computational Fluid Dynamics
SoC	State of Charge
ISC	Internal Short Circuit
UDF	User Defined Function
v	Volume
ρ	Density
C_p	Specific heat
T	Temperature
K	Thermal Conductivity
A_{mush}	Mushy Zone Parameter

T_l	Liquidus Temperature
T_s	Solidus Temperature
T_m	Melting Temperature
μ	Dynamic Viscosity
β	Liquid fraction
L_f	Latent heat of fusion
ne	Negative electrode
pe	Positive electrode
t	time
α	Degree of conversion at positive electrode
ISCD	Internal Short Circuit Device
h	Heat transfer coefficient
ε	Emissivity
Q_{heater}	Heat from heater
x	Concentration of Species
x_0	Initial Concentration
A	Frequency Factor
E	Activation energy
Kb	Boltzmann Constant
m	Mass of material at electrode
H	Enthalpy
jr	Jelly roll
V	Voltage
C	Ampere hour
Q_{flux}	Heat flux

List of Figures

List of Tables

Chapter 1

Introduction

Internal Combustion (IC) Engines are dominating the automobile industry from its inception. These engines produce power from fossil fuels such as Petrol, Diesel etc. Also we know that the reserves of fossil fuel are diminishing day by day and extraction of these fuels is becoming difficult. Another problem associated with IC engines is its emissions. For this reason air quality is deteriorating and we are facing numerous environmental and health hazards. So, we are moving towards a generation of Electric Vehicles (EVs). It has the capability of mitigating the drawbacks of IC engines. Apart from being environment friendly and battery driven EVs also has its own advantages like lower running cost, better driving experience, lower maintenance cost, reduced noise pollution etc. Hybrid Electric Vehicles (HEVs), Plug-in Hybrid Electric Vehicles (PHEVs), and Battery Electric Vehicles (BEVs) are all examples of Electric Vehicles (EVs).

A Lithium-ion battery (LIB) pack is the main power source in the BEVs. The battery pack runs an induction motor via an inverter which converts the DC output power of the battery pack to AC power to run the induction motor. An IC engine produces usable torque and power output only within limited speed range whereas in electric vehicles just by varying frequency of the power supply, we will be able to alter the drive wheel speed. So, an induction motor will work efficiently in any speed range. For this reason, induction motor has a higher power to weight ratio. However, the power supply for an induction motor is the real bottleneck for achieving a major industrial revolution in the automobile industry.

LIBs are an attractive energy storage device for EVs because it has high energy density, high specific power, lower self-discharge rates, higher recyclability, excellent cycle life, no memory effect and light weight. These properties provided the LIB an advantage over other batteries such as lead-acid, nickel–cadmium (Ni-Cd), nickel-

metal hydride (Ni-MH) batteries. Abuse tolerance is one of the most concerning aspects for LIBs as it relates to the safety issues. Workings of LIBs are affected by temperature rise. Electrochemical operation and joule heating due to electron motion within a battery cell are the two main sources of heat generation in a battery cell. So, thermal stability of these batteries needs to be checked under various abuses such as exposure to heat, external short circuit, nail penetration, crushing and so on. So, a proper battery thermal management system (BTMS) needs to be designed to control the temperature rise in the battery pack module, otherwise it can cause Thermal Runaway (TR) which will lead to a fire hazard. TR is a term that depicts a process that is driven by a rise in temperature, which then releases energy that raises the temperature even further. TR begins when heat generation inside the battery exceeds the amount of heat dissipates to its surroundings.

Active systems and passive systems are the two primary forms of BTMS. The active system is mostly reliant on the forced circulation of a specific coolant, such as air or water. A passive system uses methods such as heat pipes, hydrogels, and phase change materials (PCM) to consume no energy and so enhance the vehicle's net efficiency.

The LIB's optimal operating temperature should be kept in between 20-50º C, with a maximum temperature variation of 5º C in the battery pack. The temperature in a battery pack operating continuously outrages the safety limit of 60º C. When the temperature rises above 50º C the battery’s lifespan is put at risk, even a single cell's immature degradation can significantly affect the battery pack's performance and efficiency. The key objective of the BTMS is to regulate the temperature of the battery's cells and so extend the battery's lifespan.

We'll start by looking at the chemistry of LIB to better understand how TR happens. In the chemistry section of LIB, we'll take a quick glance at the many components of LIB to learn how it works, including charging and discharging.

1.1 Battery overview

Batteries are devices which convert the stored chemical energy into electrical energy through electrolysis process and vice versa. Batteries that can be recharged due to the reversible nature of the electrode are called secondary batteries. Widely used secondary batteries that are used include lead-acetate batteries, LIB, nickel-metal hydride, nickel-cadmium etc. LIBs works on an interesting concept associated with metals called electrochemical potential. The electrochemical potential is the tendency of a metal to lose electrons. According to the electrochemical series Li has the highest tendency to lose electrons and this makes Li a good conductor of heat and electricity.

The LIB has a cathode (positive electrode), anode (negative electrode), electrolyte, and a separator to keep the anode and cathode apart and avoid contact. Active material and current collectors make up electrodes. The current collector has the active material pasted on it. The Red-ox reaction involves active material, and the current collector serves as the conducting medium of electrons. At the anode, copper is used as a current collector, and at the cathode, aluminium is used. Binders are used to paste the active material to the current collectors.

Active material used at the cathode is mainly metal oxide, which acts as a home for the Li-ions. Li-ions are intercalated between the layered structures or the interstitial sites of the metal oxides. Metal oxides that are used in cathode should have good Li holding capability, good thermal conductivity and good diffusivity. Cathode also determines the capacity and average voltage of the battery. If the amount of Li-ion intercalated in the cathode is high that means the potential difference between the anode and cathode will also be high. Thus the capacity and average voltage of that battery will also be high. The nomenclature of various LIBs depends on the type of metal oxides used at the cathode. For example, In $LiCoO_2$ (Li-Cobalt batteries) Li-ions are intercalated in between the layers of CoO_2 (Cobalt oxide). Similarly some other types of LIBs are $LiFePO_4$ (Li-Iron Phosphate), $LiMn_2O_4$ (Li-Manganese Oxide), $LiNiMnCoO_2$ (Li-Nickel Manganese Cobalt Oxide), $LiNiCoAlO_2$ (Li-Nickel Cobalt Aluminium Oxide), $Li_4Ti_5O_{12}$ (Li-Titanate) etc.

Similar to cathode, active material is also used at the anode. In most of the cases, graphite is used as active material at the anode. Graphite has a layered structure. These layers are loosely bonded so the separated Li-ions can be stored or intercalated very easily there. Graphite is used as active material in anode as it has low electrochemical reactivity, high thermal and electrical conductivity.

Electrolyte is a Li salt-based solution that acts as a medium of movement for the Li-ions between the cathode and anode. For producing electricity the path of the electrons and the Li-ions should be different. Electrolyte is the compound which only allows the Li-ions to pass through it, not the electrons. Thus, the electrons flow through the external circuit and produces electricity. A good electrolyte should have good chemical and electrochemical stability, high Li-ion transport capacity, excellent electronic insulation performance etc. Some commonly used electrolyte materials are $LiPF_6$, $LiClO_4$, and $LiAsF_6$ etc.

To avoid short circuit between anode and cathode due to temperature rise an insulating layer called separator is placed between the electrodes. The separator is permeable for the Li-ions because of its micro porosity. If temperature rises beyond a certain limit the electrolyte may melt out, then the LIB becomes vulnerable to TR. So, separator acts as a safety barrier. Some common materials used commercially as separator are polypropylene (PP), polyethylene (PE).

The electrolyte will be degraded if the electrons come into contact with it. However, the electrons never come into contact with the electrolyte due to the solid electrolyte interface (SEI). When we charge the cell for the first time the Li-ions move through the electrolyte, in this journey the solvent molecules in the electrolyte cover the Li-ions. When they reach the graphite layer the Li-ions along with the solvent molecules form a layer there called the SEI layer. The formation of this SEI layer is a blessing in disguise. It prevents any direct contact between the electrons and the electrolyte thus saving the electrolyte from degradation. The formation of SEI layer consumes 5% of the Li, the rest 95% of the Li contributes to the main working of the battery. SEI layer irreversibly consume Li and the electrolyte, thus reducing the overall quantity of Li and thereby reducing the max capacity of our battery.

1.2 Working of LIB

Only one electron is there in the outermost shell of a Li atom and it always wants to lose this electron for gaining stability as noble gases, for to this reason, pure Li is a highly reactive metal. When there is an available path from the negative terminal to the positive terminal, this electron separates from the Li and starts heading to the other side. At the same time, the Li leaves the graphite and becomes positively or +1 charged and is now called a Li-ion. The operating principle of LIB is the fact that Li, in its pure form, is a reactive metal, but when Li is part of a metal oxide, it is quite stable. Thus we provide two different paths for the separated electron and Li-ion to flow from anode and to cathode and we get electricity because of the flow of these electrons in the external circuit. Li-ion will automatically reach the metal oxide part.

1.2.1 Charging of LIB

When we connect our power source to the metal oxide part (cathode) to charge the battery it applies a higher force on the flow of electron and the positive side of the power source will obviously attract and remove electrons from the Li-ions of the metal oxide. In case of $LiCoO_2$ battery the electrons are pulled out of the cobalt leaving them in a +4 state. These electrons flow through the external circuit as they cannot flow through the electrolyte and reach the graphite layer. Meanwhile, the positively charged Li-ions will be attracted towards the negative terminal and will flow through the electrolyte back to the graphite layers and get trapped there. Once all the Li-ions reach the graphite sheet the cell is fully charged. This process is depicted in **figure 1**.

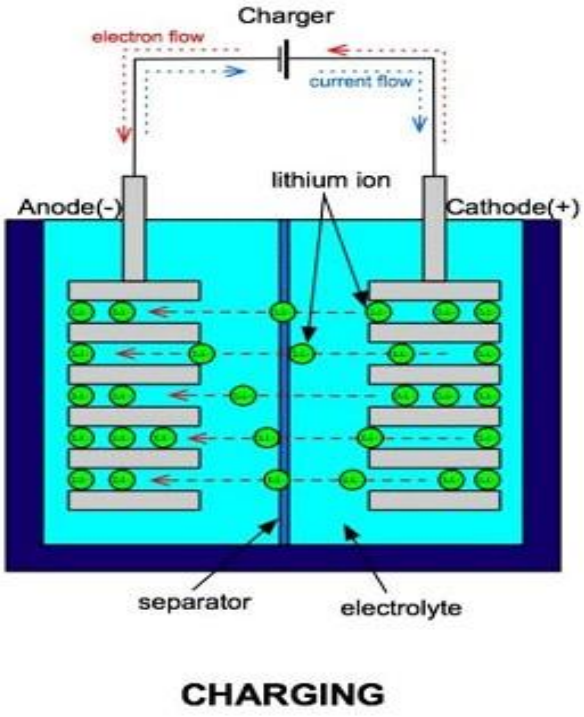

Figure 1: Charging of LIB

1.2.2 Discharging Of LIB

After the charging is done, the battery reaches an unstable state. As soon as the power source is removed and a load is connected, the Li-ions want to go back to the stable state as a part of the metal oxide. Due to this tendency, the lithium ions move through the electrolyte and the electrons via the load to the cobalt side which want to gain back in electron. We get a flow of electricity for this movement of electron in the external circuit. It can be used for various purposes. When lithium ions go to the cobalt side it again wedges itself, intercalates with the cobalt and oxygen to become LiCoO2. This process is depicted in **figure 2**.

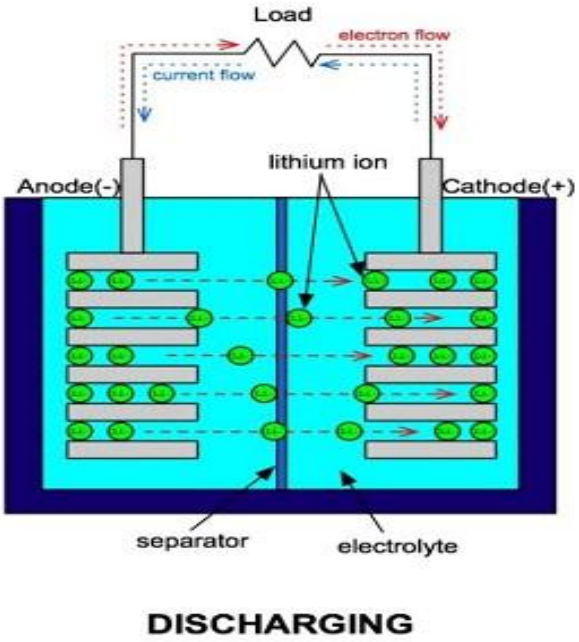

Figure 2: Discharging of LIB

Various electrochemical reactions that take place while operation of LIB at the cathode and anode during charging and discharging are:

During Discharging

At cathode: $xLi^+ + Li_{1-x}CoO_2 + e^- \rightarrow LiCoO_2$

At anode: $Li_xC_6 \rightarrow xLi^+ + e^- + 6C$

Overall equation: $Li_{1-x}CoO_2 + Li_xC_6 \rightarrow LiCoO_2 + 6C$

Reduction takes place at cathode. There, cobalt oxide (CoO_2) combines with Li-ions and forms $LiCoO_2$. At the anode oxidation takes place. There, the graphite and Li intercalated compound LiC_6 forms graphite and Li-ions.

During Charging

At cathode: $LiCoO_2 \rightarrow xLi^+ + Li_{1-x}CoO_2 + e^-$

At anode: $xLi^+ + e^- + 6C \rightarrow Li_xC_6$

Overall equation: $LiCoO_2 + 6C \rightarrow Li_{1-x}CoO_2 + Li_xC_6$

This was all about the working and chemistry behind the operation of LIB. Now we will take a look at the TR part which is a major concern of LIBs and what causes it.

1.3 TR of LIB

One of the major reasons of LIB failure is TR. It all starts when battery abuse condition occurs in one of the batteries. These abuse conditions may be electrical, thermal or mechanical. Electrical abuse occurs when the battery is over charged or over discharged. It also can occur because of high C-rate. C-rate controls the charge and discharge rates of a battery. A battery's rate of discharge in relation to its maximum capacity is measured using a C-rate. Thermal abuse occurs when the battery is overheated and mechanical abuse occurs when the car meets an accident or crash. All of these reasons result in the battery undergoing TR.

TR begins with a single cell of the battery getting heated up and breaking into fire which then slowly propagates to the remaining cells of the battery consuming the entire battery pack slowly known as thermal propagation. In general EV battery pack consists of a number of battery modules and in one such module there is also huge number of cells are confined there in small space. Due to various exothermic chemical reactions inside the battery and resistance heating (Joule heating), heat is generated inside the battery which cannot go outside of the battery pack. If there is no external method to remove the heat from the battery pack, the battery pack will build up heat and continue to get hotter, which will cause the battery to lose its rated capacity. Thus, battery deterioration consequently grows dramatically. Therefore, external cooling is essential to maintain the batteries within the optimum range of temperature.

In the beginning there is a continuous heating stage. If there is a situation when the temperature inside the LIB reaches 80-90° C, then exothermic decomposition of the SEI layer begins. Then from a stage of continuous heating the LIB enters a state of self-heating. At this time harmful gases like CO, CO_2 are liberated. Temperature increases further if attention is not given at this stage. Due to this breakdown of SEI layer, the electrolyte comes into contact with the anode and the reaction between electrolyte and lithiated graphite surface takes place, causing an acceleration of reaction at the anode. Near about 130º C temperatures, the separator starts to shrink. It causes short circuit between the electrodes and more intense reaction starts between the metal oxide at the cathode and the electrolyte. Due to this, oxygen is released, which triggers the reaction even further making the process exothermic. All these processes occur simultaneously and large amount heat and gases is released. For these reasons, the heat and gases released initiates combustion and catches fire in the LIB pack. This creates a hazardous situation. This phenomenon is known as TR of LIB. This process of TR is represented in **figure 3**.

Therefore, external cooling is mandatory to maintain the battery pack within its optimal range of temperature for safety and efficient driving of an EV. Then LIB pack can remain in safe condition as the internal heat generation and heat loss to ambient will balance each other. To alleviate the thermal problems, a proper BTMS needs to be designed to maintain the battery pack temperature as well as cell temperature to an optimal range.

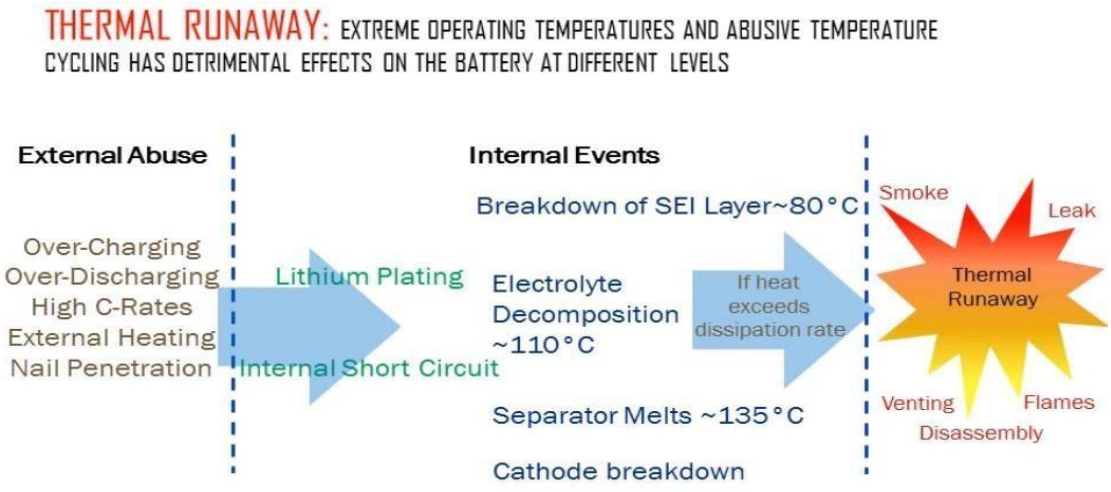

Figure 3: Representation of occurrence of TR in LIB

Chapter 2

Literature review and objective

2.1 Literature Review on Battery modelling

Hatchard et al [1] developed a predictive model for oven exposure testing using the thermal properties of the cells and reaction kinetics for the electrode materials while the electrolyte is exposed to high temperature. LIBs must successfully pass oven exposure testing before being given the go-ahead for sale by regulatory organisations. Without actually creating any cells, the model can anticipate how electrode materials and new battery sizes will react to oven exposure tests. Additionally, it would allow same testing of new electrolytes or additives. Even though, it's crucial to pay attention towards the electrolyte to electrode material ratio. The model may be used to predict the results of switching to a more reactive cathode, a carbon anode with a larger or lower surface area, and changing labels.

One dimensional formulation developed by hatchard et al [1] is further extended to three dimensions (3-D) by Kim et al [2]. In order to take into account the geometrical aspects, which is crucial for the large cells used in automotive applications, this model was built. The three-dimensional model, which is used to mimic oven tests and ascertain how a local hot spot can spread across the cell, records the shapes and dimensions of cell components as well as the spatial distributions of temperatures and materials. Depending on the size of the cell the 3-D model predicts that the TR will occur sooner or later from the lumped model compared to the oven abuse simulation testing of cells with CoO_2 cathode, graphite anode and standard $LiPF_6$ electrolyte. The outcome of this study shows that smaller cell rejects heat faster than large cells. So, to prevent TR under same abuse conditions using small cells is more beneficial. This study shows, small hot spots inside large cells initially propagate in the longitudinal and azimuthal direction.

A mathematical model by Coman et al [3] predicts the gas generation and the temperature-pressure behaviour for an 18650 LCO/Graphite cell having a Dimethyl Carbonate (DMC) electrolyte. The analysis was carried out at intervals close to the venting event and the cell was modelled using oven heating conditions. The model was created by calculating the energy balance for a control volume with unsteady flow and using the isentropic flow equations that correlate to gas venting. The outcomes demonstrate that when no gas is generated within, the model is unable to forecast the pressure as observed experimentally. The model can simulate the pressure profile observed during actual measurements when the gas generation brought on by pre-venting reactions is included.

The 18650 cylindrical LIBs transient temperature and voltage distributions at various discharge rates are predicted using a mathematical model in this research by Parekh et al [4]. In order to provide quantitative data regarding the thermal behaviour of LIBs, the 18650 cylindrical LIBs are tested inside the lab using air-cooling. Four thermocouples were mounted on the battery surface under four constant current discharge rates of 1C, 2C, 3C, and 4C. According to modelling, the greatest temperature is 46.86°C at a 4C discharge rate. The findings also demonstrate that higher C-rates raise the temperature of the battery's main surface.

The internal short circuit (ISC) device implanted in Li-ion battery cells is used in the paper of Coman et al [5]. It is an innovative model to analyse TR in these cells. The self-heating chemical reactions and the State of Charge (SoC) are represented in the model using Arrhenius formulations. An internal short circuit device in the cell windings (jelly roll) causes a local short circuit, which is taken into consideration in the model. An efficiency factor for converting electrical energy into thermal energy is added to the total amount of electrical energy that is available while modelling the short circuit. The energy released from the cell is taken into consideration by the efficiency factor. The energy released by a battery cell with an ISCD was discovered to be roughly equivalent to the energy released by a battery cell that experiences TR as a result of overheating. They discovered that TR releases 28% of the 18650's 2.4 Ah of electrical energy.

2.2 Literature Review on TR

In order to define the thermal behaviour and establish safe procedures, this work by Lopez et al [6] focuses on experimental explanation and analysis of various LIB module configurations. In the heat-to-vent setting of the abuse test, a heating element causes a single cell in a module to enter TR. It has been determined how thermal runaway propagates from cell to cell. The likelihood of TR propagation in a module of cylindrical cells is greatly reduced, according to the results, by increasing the inter-cell spacing. It also reduces cell temperatures, reduces loss of cell voltage, and lessens the harm to surrounding cells. Based on these findings, a minimum cell distance of 2 mm is advised to reduce the risk of TR propagation and module damage. Additionally, the testing revealed that branching tabs, as opposed to serpentine tabs, improve the voltage retention and safety of the modules because they better isolate the shorted trigger cell from the rest of the module electrically. In conclusion, depending on the cell type and module arrangement, different techniques should be used to reduce the likelihood of TR propagation.

Cai et al [7] describes a gas sensing-based early detection technique for LIB TR. Early identification of cell failure is feasible by measuring CO_2 concentrations, which are formed at the beginning of battery TR. In comparison to traditional surface temperature sensing, the simulation demonstrates a significantly faster response time for gas sensing. The gas sensing approach predicts the event before TR propagation, in contrast to the surface temperature sensing strategy, which fails to identify TR before it spreads to neighbouring cells. The outcome indicates that after 710 seconds of the first TR event, nearby cells will start a TR, and this period is known as the key time for TR propagation. To prevent further risks from TR propagation, early detection made before propagation critical period is required. TR cannot be detected before 710 seconds using drum surface temperature measurement. By switching to gas sensors, it is possible to detect TR 85 seconds earlier than the propagation critical time. The findings indicate that while employing the gas sensing technology suggested in this paper will enable early detection of TR and drum surface temperature detection is too slow for TR detection.

Feng et al [8] gives a comprehensive review of the commercial LIB for electric EVs' TR mechanism. The energy release diagram with two examples is used to further clarify the relationship between the ISC and the TR. A three-level protection approach is suggested to aid in lowering the TR hazard. By providing passive defence and early warning before the occurrence of TR, by improving the materials' intrinsic thermal stability, and by minimising secondary hazards like TR propagation, the three-level protection can be achieved. The most common feature of all abuse scenarios is the ISC. Different forms of ISC correspond to various abuse scenarios. The spontaneous ISC evolves over the course of the battery's whole cycle life and is currently thought to be the hardest challenge to overcome. When the self-discharge rate and exotic heat generation are taken into account, there are three levels of ISC. Early detection needs to start working before the ISC progresses to the third level, or TR. To measure the reaction kinetics for all the constituent components inside the cell during TR, a novel energy release diagram is presented. The proposed energy release diagram quantifies the energy released by combustion, ISC, and chemical processes. The proposed energy release diagram explains the chain processes during TR in detail. There are three stages at which the TR hazard reduction can be accomplished. First, via material change, increase the intrinsic safety of anti-TR features; second, set passive protection against real-world abuse conditions; and third, build early warning algorithms before TR. This will provide the passenger enough time to escape the EV in the event of an accident.

Wang et al [9] showed a variety of electrode materials, electrolytes, and cell types exhibit various TR behaviours, and it is being investigated exactly how these reactions change depending on the materials used for the cathode, anode, and electrolyte components. The SoC, discharging rate also heavily influence the reactions. Using Finite element method (FEM) and Finite volume method (FVM) techniques, thermal models from one dimensional to three dimensional have been built and simulated. Using one or more safety devices in conjunction with the inherent safety approach is currently an effective way to stop battery explosions. Future studies should take into account extreme situations for example when the engine will start battery will produce high discharge rate.

2.3 Literature Review on cooling methods

Temperature has a significant impact on the functionality and lifespan of LIB. For safety, performance capacity, and lifespan, the battery should be stored in an environment with properly regulated temperature and no possibility of TR. According to Pesaran et al [10] BTMS needs to do four tasks to keep the battery pack in optimum condition. They are cooling, heating, insulation and ventilation.

Both power and heat are created when a battery cell is operating. To maintain ideal conditions, we must dissipate this heat to ambient in advance. BTMS must therefore use a cooling technology.

An unfavourable environment for batteries is one where the battery pack temperature drops even lower than the lowest optimal temperature limit. Therefore, we require a heating system, such as a Positive Temperature co-efficient (PTC) heater, to quickly raise the battery's temperature to its ideal working range.

The temperature difference between the interior of the battery pack and the outside environment is greater in extremely hot or cold environments. Therefore, there is a potential that the temperature will decrease or rise outside of its proper temperature range in such situation when the battery is not functioning, for instance while the car is parked. As a result, it is quite challenging to get the battery up and running in a short amount of time. Therefore, the battery pack needs to have adequate insulation.

There's a potential that a battery pack's internal chemical reactions will produce gas, which needs to be vented outside of the battery pack. So, ventilation is needed.

The key objective of BTMS is to maintain temperature gradient, which can result in uniform heating between the batteries in the LIB pack, while minimising the highest temperature reached and the temperature difference between batteries in a LIB pack. Numerous studies have recommended that the maximum temperature limit should be within 40°C and that the maximum temperature variation within the LIB pack must not exceed 5 °C. In addition, BTMS needs to be lightweight, affordable, simple to maintain, and extremely reliable.

2.3.1 Classification of LIB cooling systems:

We have previously discussed the operations that take place in BTMS of an EV. Now, we will discuss the various cooling techniques that are used to reduce the temperature of a battery due to heat generation. Classification of LIB cooling can be done by the following methods discussed in **figure 4.**

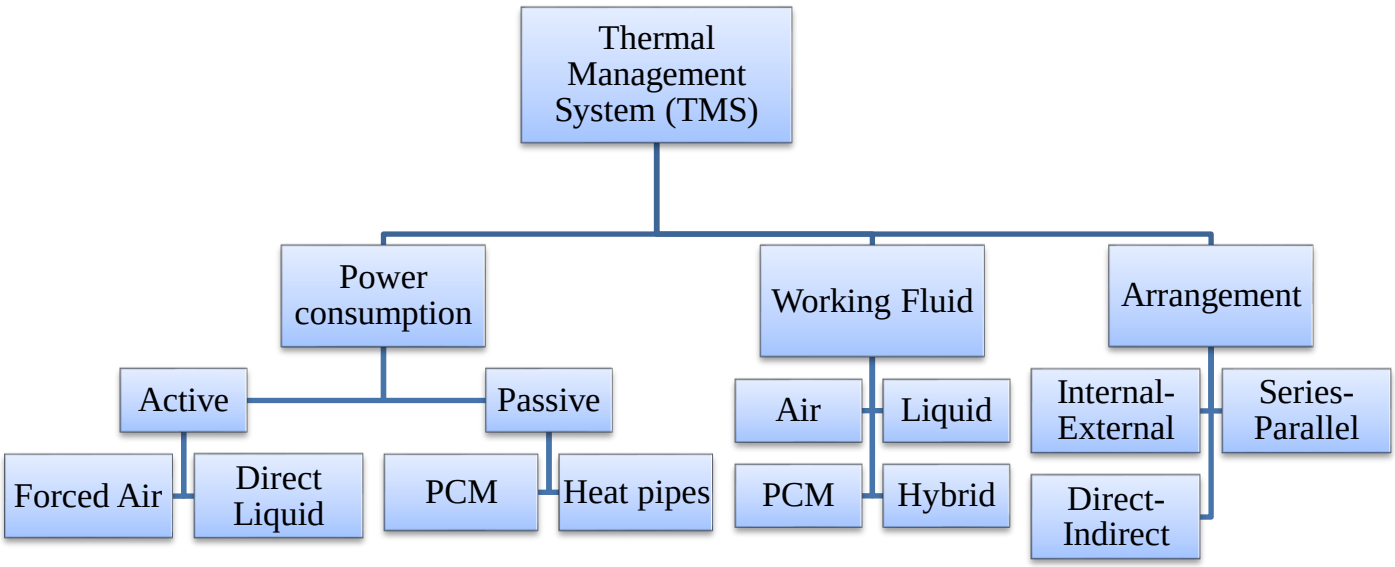

Figure 4: Classification of BTMS

They are based on-

1. Power consumption i.e. active cooling and passive cooling.

Active cooling describes cooling techniques that depend on external device to improve heat transfer. Through active cooling method, the rate of fluid flow increases which further increases the convective heat transfer. Active cooling solutions include forced air through a fan or blower, direct liquid, jacket cooling and cold plate which can be used to optimise thermal management system.

In passive cooling technique energy requirement is very less and ambient condition is used as a heat sink. Due to their energy efficiency and lower cost, passive cooling solutions are a wise system design choice for the thermal management of both EV and electronic devices. Passive cooling techniques includes phase change material (PCM)

cooling and heat pipe cooling. By deploying a heat spreader or a heat sink to maximise the radiation and convection heat transfer modes, passive cooling achieves high levels of natural convection and heat dissipation.

2. Working fluid, which includes air cooling, liquid cooling, PCM cooling and hybrid cooling. Hybrid cooling is achieved when two or methods (or working fluid) of cooling is used as a combination.

3. Arrangement i.e. depending on the positioning of the cooling system in array. They can be of three type's internal-external, direct-indirect and series-parallel.

Example of internal cooing is by using electrolyte as a coolant through micro channels, internal cooling channel that circulates water through the battery cells. External cooling medium is most popular. It is achieved when the battery is cooled using an external coolant like air or liquid coolant.

Direct or indirect cooling system is classified on the basis of whether the cooling medium is in direct contact with the LIB or not. If it has a direct contact then it is direct cooling otherwise it is called indirect cooling.

Series and parallel stands for different cooling circuits that are used in LIB cooling. Depending on the situation type of cooling circuits is determined.

These classifications of thermal management system are explained in the review work of Tete et al [11]. Now we will look at the different cooling methods and their literatures.

2.3.1.1 Air cooled BTMS

BTMS uses an air cooling system because of its straightforward construction and low maintenance requirements. Air from the evaporator, preconditioned air from the cabin, and ambient outside air can all be used as a cooling source. The air source is chosen based on heat generation, ambient conditions, and driving tendency. Air cooling systems are less efficient because of their low thermal conductivity and low heat

capacity. Other drawbacks of this system include its limited capacity for batteries due to the need to maintain an appropriate air space between batteries. The system is huge and noisy because it uses an integrated system of ducts and fans to circulate a large volume of air for effective cooling. To enhance the cooling system's performance, research is being done. To increase the system's efficiency, changes are made to the cell configuration, airflow pathways, and air channel design.

Park et al [12] theoretically investigates and numerically models a specific design of an air-cooled battery system to meet the necessary thermal parameters. Since a HEV's conventional battery system is made up of many battery cells that are stacked one on top of the other, the uniform distribution of air flow circulation in the coolant passage, which dissipates heat produced by the battery cells, determines cooling performance. It is shown that the desired cooling performance may be attained even with the current battery system's layout and design unchanged by using the tapered manifold and pressure relief ventilation. The thermal resistance model, which can categorise the various heat transfer mechanisms, is used to analyse the cooling performance. The proposed tapered manifold and pressure relief ventilation are used to accomplish the needed cooling performance while taking into account the restrictions for the air flow arrangement. Also, release of air pressure reduces the electricity needed to run a fan.

For EV applications, a transient numerical model of a LIB pack with an air-cooled thermal management system was developed by Cho et al [13]. The internal resistance map based on experiments and the open circuit voltage is both employed in the battery model. For estimating activation voltage loss, the Butler-Volmer equation is taken into direct consideration. Different ambient temperature conditions are used to model the impacts of the module configuration. The temperature difference between the modules increased at a low ambient temperature and decreased at a high ambient temperature in all arrangement conditions in the battery pack. Furthermore, in all ambient conditions, the module configuration has a significant impact on temperature deviation. Regardless of the ambient temperature, the temperature difference between

modules in a battery pack is reduced more significantly when they are arranged so that more cells are close to the air intake.

The study by Lu et al [14] aims to investigate the impact of air cooling on temperature uniformity and hotspot mitigation of a small battery pack under different air flow pathways and airflow rates. The numerical results demonstrate that a reduction in the maximum temperature and an improvement in the maximum temperature difference in the densely packed battery box may be achieved by increasing the effective heat transfer regions between the battery surfaces and the air-coolant. The result suggests that as cooling channel sizes increase, the maximum temperature eventually decreases. Also, the increase in cooling channel diameters causes a progressive decline in the maximum temperature's decrease degree, demonstrating that this approach to reducing the maximum temperature is not the best one.

The arrangement of the battery cell spacing for better cooling performance is used in this work by Chen et al [15] to optimise the configuration of the LIB pack in parallel air-cooled BTMS. An optimisation strategy for the battery pack is suggested using flow resistance network model and heat transfer model combined, with a constant cell heat generation rate. After optimization, the BTMS' cooling performance is noticeably better. After optimization, the maximum temperature difference is decreased by 42% and the maximum temperature of the battery pack is somewhat lowered, but the system's overall pressure loss remains unchanged. Furthermore, even with different input flow rates and in the case of an unstable heat generation rate, the modified BTMS still outperforms the original one. According to the optimization method, the spacing should be adjusted so that it is greater around the LIB with the highest temperature and smaller around the one with the lowest temperature.

Experiments and computational fluid dynamics (CFD) simulations are used to study in the work of Xie et al [16] the effects of three parameters (the air-inlet angle, the air-outlet angle, and the breadth of the air flow channel between LIBs) on the heat dissipation of a LIB pack. Then, the single factor analysis and orthogonal test approach are used to optimise the three structure parameters. The conditions of 2.5º air-inlet angle, 2.5º air-outlet angle, and equal channel width result in the best cooling

performance. The maximum temperature and the temperature differential are reduced by 12.82 % and 29.72 %, respectively, using the optimization method.

2.3.1.2 Liquid cooled BTMS

Liquid cooling of LIB can be achieved in two ways direct and indirect cooling. Liquid cooling has high cooling efficiency than air cooling. It provides uniform temperature distribution across LIB pack. Overall liquid cooling gives continuous and stable cooling performance. These are the advantages of liquid cooling system. The disadvantage of liquid cooling system is associated with its cost. High mass cost required for the equipment that are required to design the liquid cooled system. It also has high maintenance cost.

In direct type of liquid cooling battery is submerged directly into the coolant. In this type of cooling the coolant must have low to no conductivity to maintain vehicle safety. Though it has excellent cooling potential, it is not yet commercialised for EV use as it is under continuous research and development.

In indirect cooling system the coolant circulates through system of pipes. It is also similar to the cooling system that we can observe in IC engines. In this type of cooling the coolant must have high heat capacity along with corrosion inhibiters. It is the most promising cooling system in the market.

At varying galvanostatic discharge rates of the battery pack, a transient mathematical model taking account for the conservation of charge, species, and energy for a lithium-ion bipolar battery pack is solved by Tong et al [17]. The temperature window within which the pack will operate at different discharge rates is identified after identifying two limiting situations with and without cooling. With a minimum cooling condition of 1 C, 2 C, and 5 C-rate, respectively, it is discovered that 45, 22 and 7 stacks at the module level of the pack may be put between the coolant plates with an average temperature less than 313 K. A trade-off between these parameters should be

made since increasing coolant velocity and coolant plate thickness helps to manage the maximum temperature and temperature non-uniformity, but doing so also increases the parasitic load and adds to the pack's weight and volume.

In this research by Qian et al [18], a three-dimensional numerical model was created using a type of liquid cooling technique based on mini-channel cold-plates to investigate the thermal performance of LIB packs. On the thermal behaviours of the battery pack, the impacts of the number of channels, inlet mass flow rate, flow direction, and channel width were examined. The findings demonstrated that the mini-channel cold-plate thermal management system was effective in reducing battery temperature at 5C discharge by providing good cooling efficiency. It was sufficient to use a 5-channel cold plate, and it was clear that increasing the incoming mass flow rate would reduce the temperature.

In this study by Li et al [19], experimental and numerical investigations are conducted to explore the thermal performance of water cooling based BTMS in LIBs dynamic cycling. An electrochemical-thermal model is used in numerical simulation to predict the thermal behaviour. The voltage, current, and temperature distribution in the individual battery and battery pack are presented for both experimental and simulated findings. Additionally, the active water cooling system is the superior technique for enhancing the thermal performance of the battery pack at low cycle rates. Additionally, a compound system needs to be designed in the actual battery pack system to deal with the circumstance of using battery packs in a variety of ways and at various rates.

Chen et al [20] gives a comprehensive method for quantitatively assessing a liquid-cooled battery module's cooling performance. Using experimentally determined thermal parameter values, the fluid-solid coupled heat dissipation model is created using CFD. The Latin Hypercubes approach is used to create parameter combination samples, and sensitivity analysis is used to determine how structural characteristics affect heat dissipation performance. The development of a cooling system with a lower temperature and less energy consumption is then accomplished through multi-objective optimization. Implementing the suggested method in the production of

industrial battery packs is simple. The results demonstrate that the temperature reduction will be greater with the same input power, 1.87 °C, and that the temperature deviation can also be regulated within a narrow range, 0.35 °C.

2.3.1.3 PCM cooled BTMS

PCM is a term used to describe a substance that can either absorb or release latent heat to maintain a temperature that is nearly constant. While liquid cooling BTMS requires complicated devices to ensure the effect, the classic air-cooling based BTMS not only demands extra power but also is unable to fulfil the demand of modern LIB packs with high energy density. As a result, PCM-based BTMS is growing popular. The temperature of a battery pack could be maintained within the typical working range for a long time without requiring any external power by utilising PCM to absorb heat. By combining with fillers that have high thermal conductivity, like expanded graphite and metal foam, or by combining with fins, PCMs could significantly increase the heat dissipation efficiency of BTMS. Due to its low cost, easy equipment, and high cooling efficiency, the PCM cooling method is typically regarded as the most suited one for BTMS when compared to the conventional air cooling, liquid cooling, and heat pipe cooling.

2.3.1.3.1 Classification of PCM

There are numerous different PCM classification standards. PCMs can be loosely categorised into solid-solid PCMs (SSPCMs), solid-liquid PCMs (SLPCMs), solid-gas PCMs (SGPCMs), and liquid-gas PCMs (LGPCMs) based on the phase of the substances before and after the changing process. SLPCMs fall into the most widespread application sector among them due to its huge latent heat capacity, small volume change during the phase changing process, and ease of access to raw materials. They are discussed in **figure 5.**

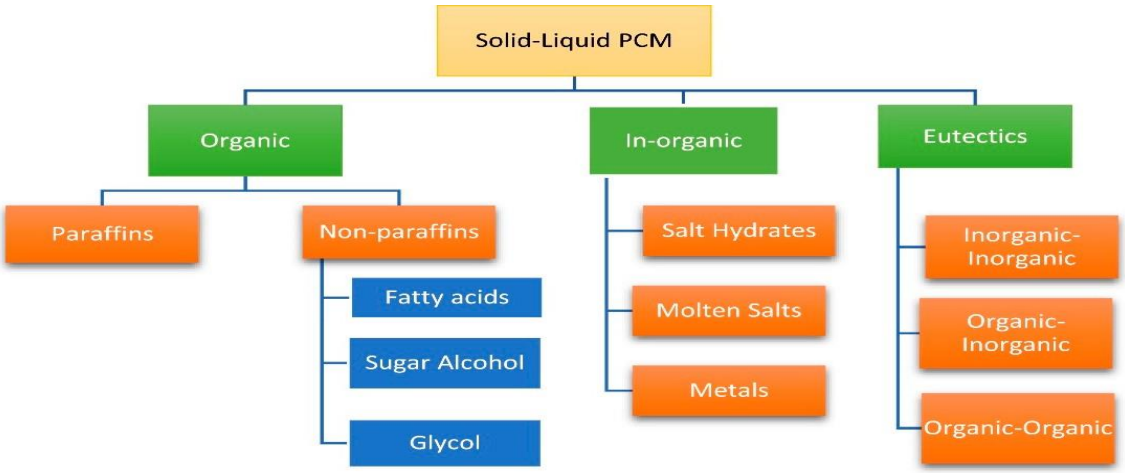

Figure 5: Classifications of PCM [21]

This generalised category of PCM is taken from Lieu et al [21]. Organic PCMs mostly refer to paraffin and non-paraffin compounds, which include stearic acid, polyols, long-chain alkanes, and other non-paraffin substances. Organic PCMs have been the primary source of PCM raw materials because of their advantages in terms of corrosion resistance, safety, nontoxicity, good chemical durability, and almost no super cooling. They do, however, also have drawbacks including poor heat conductivity and easy phase change leakage.

Water, hydrated salts, melted salts, and metal are the main components of inorganic PCMs; hydrated salts and metal are particularly popular. They are non-flammable, non-leaking, have a high latent heat capacity, and are reasonably inexpensive. The widespread application of hydrated salts is severely constrained by their corrosive nature, ease of phase separation, and super cooling.

Eutectic PCMs are crystal mixtures of several soluble components that could be characterised by simultaneous melting and solidification. Their melting point and freezing point are typically lower than those of pure substances. Eutectic PCMs are typically prepared by combining two or more substances with low melting temperatures, including organics, inorganic compounds, or both inorganic and organic compounds.

2.3.1.3.2 Selective conditions of PCMs

The selections are basically done on the following aspects.

1. The PCM phase transition temperature is within the usual operating temperature range.

2. Thermodynamic properties i.e. good thermal conductivity, high latent heat of fusion per unit volume, great specific heat, low degree of super cooling and high density. They should also have small volume changes on phase change and strong ability to absorb heat and get latent heat.

3. They should have good chemical stability, good corrosion resistance, non-toxic and inflammable.

4. It should have large scale availabilities, low cost and no leaking tendency.

5. It should have some kinetic properties like high nucleation rate and high rate of crystal growth.

2.3.1.3.3 Table 1: Enhancement of PCMs with Different Improving Methods

Ways	Advantages	Disadvantages
Adding fins	Simplify the operation process, materials can be obtained easily, high efficiency of heat dissipation	Large contact thermal resistance, high cost, poor refill ability, large volume
Adding fillers	Low cost, improved latent heat, easy availability of materials	Easy to be aggregated and precipitated, insufficient thermal uniformity in BTMS
Encapsulation	Good strength, great flexibility, good corrosion resistance, superior sealing performance, high safety	High technological demand, high requirements for packaging materials.

Recently, pure PCMs were unable to fully satisfy all application requirements due to some drawbacks such super cooling, poor thermal conductivity, and chemical instability. Therefore, researchers' primary interest in the performance and uses of PCMs is in ways to increase thermal conductivity. As PCMs have evolved, many techniques have been used to increase their thermal conductivity in accordance to the industry's increasingly stringent standards.

The three most important techniques at the moment are adding fins, packaging technology, and adding high thermal conductivity fillers. Due to its low cost and simplicity of use, the approach of adding fillers has taken over as the main modification method. Various techniques for increasing thermal conductivity are discussed in the table above, with each method's advantages and disadvantages highlighted [21].

In this work by Hallaj et al [22], a novel PCM-based thermal control system for EV batteries was introduced and examined. The temperature rise of the module using the PCM was much less than that of the identical cell under the same cooling conditions, according to simulation data. It is expected that the temperature rise will be less for the 100 Ah cell with medium to high heat-transfer coefficients than for the cells in the module with a PCM thermal management system. However, the temperature difference between the cell core and surface in 100 Ah cells is large at high cooling rates (for instance, h=100 W m^2 K^{-1}).

Khateeb et al [23] found results for a LIB sub-module with nine 18650 Li-ion cells encased in PCM with a melting point of 41 to 44 °C. To address the PCM's low thermal conductivity and low natural convection heat transfer coefficient, aluminium foam inside the PCM and fins attached to the battery module were examined. The PCM's poor thermal conductivity makes it ineffective at heat dissipation, according to simulation results of the LIB module using PCM alone. With the inclusion of aluminium foam along with the PCM, the temperature rise in the battery was 25^0 C less. The LIB module demonstrated a temperature rise of 25 °C during summer

operation, from an initial temperature of 40 °C, which is a safe temperature range for the LIB module. Under the winter operating conditions with a 0 ^{0}C start temperature, the PCM did not melt.

Extreme conditions, such as a discharge rate of 2.08C-rate (10A) and an ambient temperature of 45^{0}C, are tested on a passive thermal management system for LIBs using PCM by Kizilel et al [24]. High energy packs using PCM are discharged safely at high currents and have a capacity degradation rate that is half that of LIB packs without thermal management systems. Additionally, the compactness of the packs reduces the overall weight for big power applications.

Rao et al [25] discusses the thermal energy management capabilities of aged commercial rectangular $LiFePO_4$ power batteries using PCM as well as thermal behaviour linked to thermal conductivity between the PCM and the cell. According to the experimental findings of the cells discharged at 35 A (5C). The formulation of individual cells and battery pack 3-D modules is done separately. The findings demonstrate that a temperature differential is inevitably caused by the thermal resistance in the cell. To increase heat transfer, it is important to increase the PCM's thermal conductivity and decrease its melting point. With a desired maximum temperature below 50 C, the PCM with a melting point lower than 45 C will be more efficient at dissipating heat. Significantly less temperature difference will exist throughout the entire unit prior to PCM melting. Additionally, a suitable k_{pcm}:k_c is required for a well-designed BTMS.

Javani et al [26] uses PCMs surrounding the cells that are varying thicknesses. The orthotropic feature of Li-ion cells improves the planar heat transmission and efficiency of the PCM around the cell, despite the limited peripheral surface of the LIB. The outcomes demonstrate that the use of PCM lowers the maximum temperature and temperature variation in the cell. The temperature is lowered by 3.0 K with a PCM that is 12 mm thick. The equivalent values are then determined to be 2.8 K, 2.9 K, and 3.0 K for layers that are 3 mm, 6 mm, and 9 mm in thickness. Furthermore, when the cooling system is in transient condition, the PCM's impact on the cell temperature is more pronounced. The temperature distribution becomes

around 10% more uniform when a 3 mm-thick PCM is used for the Li-ion cell, which is a significant outcome for thermal management systems in electric vehicles.

Goli et al [27] demonstrate how hybrid PCM with graphene fillers may significantly enhance thermal management and LIB reliability. The hydrocarbon-based PCM can have its thermal conductivity increased by more than two orders of magnitude by adding graphene while keeping its capacity for latent heat storage. The temperature rise inside a typical LIB pack is significantly reduced due to the sensible and latent heat storage as well as better heat conduction outside of the battery pack.

Greco et al [28] examines the PCM/compressed expanded natural graphite (CENG) thermal management of a cylindrical battery cell. Additionally, the PCM/CENG cooling strategy's maximum temperature is considerably lower than the forced convection's in the same arrangement. During the melting process, the PCM cooling can maintain a lower maximum temperature while extending the transient time for temperature rise.

2.3.1.4 Heat pipe cooled BTMS

A heat pipe is a device that can transfer heat spontaneously, without the need for any additional power sources. It is made up of an evaporator, an adiabatic, a condenser, and a wick. The heat point (heat source) where the liquid working fluid of the heat pipe absorbs sand evaporates is connected to the evaporator portion. Due to the internal pressure differential, the evaporated working fluid then travels via the adiabatic portion to the condenser section. The working fluid exchanges heat with the condenser's heat exchanger before condensing. The working fluid is once more carried to the evaporator by the capillary action of the wick after becoming a liquid. This is how a heat pipe functions. The system is generally compact, has low flexible geometry, and requires little maintenance. However, due to the limited contact area, poor capacity, and consequently low effectiveness of this technology, it is not utilised in the LIB thermal management system of EVs.

The thermal management system with heat pipes was created by Rao et al [29] in accordance with the heat generated character of batteries in order to prolong the cycle duration of batteries and lower the total cost of EVs. The outcome of the experiment demonstrated that when the heat generation rate was less than 50 W, the maximum temperature could be regulated below 50 C. The heat generation rate shouldn't be higher than 30 W when combined with the desired temperature difference.

To simulate the heat and mass transfer between heat pipes and batteries in this study by Li et al [30], the TR model is coupled with the Volume of Fluid (VOF) model of heat pipe cooling and solved in ANSYS FLUENT. The heat and mass transfer in the VOF model throughout the TR process is calculated using a user-defined function (UDF) code that includes a mass source and an energy source. To investigate the TR processes of a single battery under various operating situations and the TR propagation from a battery to adjacent batteries, numerical simulations are used. The TR of a single battery cannot be prevented by the heat pipe cooling system, but it can be prevented from spreading from a battery to nearby batteries.

2.3.1.5 BTMS using thermoelectric current

A specific temperature range is where LIBs work at their finest. Heating batteries reduces their performance in equatorial and subtropical regions, whereas freezing climates prevent batteries from functioning effectively. Thermoelectric elements used by BTMS enable the heating and cooling of LIB in accordance with requirements.

Applications for thermoelectric elements can be divided into two categories. The Seeback effect, which turns heat into electricity, is the basis of the first one (Thermo electric generator: TEG). The second, on the other hand, is based on the Peltier effect, which transforms electricity into helpful impact for cooling or heating (Thermo electric cooler: TEC). Prior to this time, TEC used for heating and cooling purposes as well as to give passengers comfort in several vehicle industries. Once this was realised, BTMS started to use it. P-type and n-type semiconductors make up TEC. The cold side of the TEC is connected to the LIB for BTMS purposes, and the hot side is

connected to the heat sink—typically a cold plate—through air or cooling liquid. For TEC to function, direct current (DC) is applied. Heat moves from the heat source side (LIB) and transmits to the cold plate side as DC is supplied to the hotter side, cooling the LIB. TEC creates a heating effect while changing the current's direction. Therefore, depending on what is needed for LIB functionality, either a heating or cooling affect can be created using the same TEC. In addition, the amount of DC supply can be adjusted to manage the degree of heating and cooling.

Above discussed methods are the widely used cooling strategies that are used and also some of them are under research. In addition to this, researchers have also looked into other methods for improving BTMS design.

The TR expansion research of nine-palace grid glass fibre partition packaging was investigated by experiment and computer simulation by Qin et al [31] in order to enhance the safety performance of 18650 LIB in storage and transportation. The findings demonstrate that the glass fibre barrier may successfully prevent the TR expansion of LIB when there is certain spacing between the batteries and the partition. The partition's thickness is 1.2 mm, and 2.2 mm is the ideal gap between the battery and the partition. The battery's surface only reaches a maximum temperature of roughly 130 degrees under ideal conditions. Using the optimum glass fibre partition packing can considerably increase the safety and protection capabilities of a LIB.

The impact of water mist (WM) on TR has been examined through a number of tests in this study by Liu et al [32] because it is a healthy and effective cooling method. An electric heater was used to warm batteries at different SOCs to induce TR, and surface temperatures were monitored throughout the testing. It was discovered that applying WM before reaching the threshold temperature can delay the onset of TR. When the temperature is 20°C to 30°C or less than the SoC's threshold temperature for TR, WM must start to manifest. However, it was also shown that if the temperature approaches the critical level, WM cannot stop TR.

Reading through the literature, we discovered that scientists have used experimental and numerical analysis to discover a number of strategies for the early identification

of the TR in LIB. Because we constantly have to destroy batteries to obtain data for analysis, experimental analysis for researching TR in LIB is not financially viable. In actuality, when doing an experimental analysis, we obtain data for analysis at a few particular locations. These factors led to an increase in the use of numerical TR analysis on software platforms like COMSOL, ANSYS, etc. A numerical investigation is inexpensive and allows us to determine the values of many unknown variables across the board.

2.4 Objectives of the present work

The available literature makes it quite evident that significant experimental and computational work has been done in the area of BTMS. The trade-off between various cooling approaches, such as liquid cooling, PCM cooling, and air cooling, has already been the subject of extensive research. Numerous studies have been conducted to lower the power requirement and reduce the size of the battery pack. We discovered that PCM-assisted battery cooling is currently of great interest to researchers.

This report mainly focuses on PCM cooling under a single battery and we will also capture the intermittent behaviour of PCM using the commercial software ANSYS FLUENT 16. Here we have taken an 18650 $LiCoO_2$ LIB for the battery simulation and Lauric acid as the PCM.

The following objectives are fulfilled and presented in this thesis:

1. To see the effect of h on battery temperature and melting runtime under constant heat generation
2. Melting and solidification behaviour of PCM under constant heat generation.
3. To investigate effects of air cooling and PCM cooling on a single battery where battery is under TR.
4. Safe condition or zone of operation for a given configuration of an 18650 battery at a given C-rate during PCM cooling.

Chapter 3

Numerical modelling

3.1 Battery modelling

When it comes to simulating TR in LIB, LIB modelling takes the prime focus. We have discussed earlier in the section 1.1 and 1.2 that both the chemistry part as well as heat transfer part needs to be understood in order to model the LIB. Therefore, to model LIBs and solve its problems, we need a multidisciplinary engineering approach.

The temperature inside the LIB will vary spatially and over time in the case of a 2-D simulation. In order to obtain temperature variation, the generalised 2-D heat transfer equation is the essential equation that is solved in ANSYS. The heat transfer equation is represented as,

$$\frac{\delta}{\delta x}\left(k\frac{\delta T}{\delta x}\right) + \frac{\delta}{\delta y}\left(k\frac{\delta T}{\delta y}\right) + Q_{gen} = v_{cell} * \rho_{jr} * C_{P_{jr}} * \frac{dT}{dt} \quad \text{..... (1)}$$

Except for the heat generation term, which is the main subject of our attention, all the terms in the equation above are well-known. TR of batteries is influenced by the temperature and reaction rate at the electrodes because these reactions generate internal heat within the battery. It is a transient heat transfer phenomena as well. In the case of LIB, the disintegration of various components starts as soon as the battery temperature reaches a specific threshold value. Additionally, the pace of reaction between the Solid Electrolytic Interface (SEI), Positive Electrode (PE), Negative Electrode (NE), and State of Charge (SoC) affects heat generation. The decomposition of several constituents was observed to follow the Arrhenius formulation. Therefore, the sum of the heat generation occurring at SEI, NE, PE, and due to short circuit can be used to indicate net heat generation due to thermal degradation, and it is represented by the following equation.

$$\mathbf{Q_{gen} = Q_{sei} + Q_{ne} + Q_{pe} + Q_{soc}} \quad \text{..... (2)}$$

The total of heat produced within LIB and heat exchange with the environment is the net heating rate. Convection and radiation are used to exchange heat with the environment. If the rate of heat generation is greater than the rate of heat dissipation to the environment, heat accumulates and temperature rises, leading to TR.

In this chapter, we'll learn about the heat generating terms—Q_{sei}, Q_{ne}, Q_{pe}, and Q_{soc}—which are the main reasons for TR occurrence. Then with the help of these heat generation terms a zero dimensional model is developed and simulated in ANSYS FLUENT 16 software. We observed that our temperature vs. time data was in good agreement with the literature [5]. Then with the help of the model developed, we will see the effect of air cooling and PCM cooling on it.

At any given time step, we must obtain concentration in order to determine the heat generation related to each LIB component. Therefore, we have used the Species Transport Equation (SPT), in order to achieve this goal and execute simulation in ANSYS, which can be expressed as,

$$\frac{\delta \rho \varphi_k}{\delta t} + \frac{\delta}{\delta x_i}\left(\rho u_i \varphi_k - \Gamma_k \frac{\delta \varphi_k}{\delta x_i}\right) = S_{\varphi_k} \ldots\ldots\ldots\ldots\ldots\ldots (3)$$

1st 2nd 3rd 4th

Where, the first term indicates the unsteady term, the second one is the convective flux, the third one is diffusive term and the fourth is the source term.

3.1.1 Governing equations of battery

As previously said, we are aware that heat is produced as a result of a reaction involving Li metal. We will now study equations for the rate of reaction and heat production caused by reactions. Due to these processes, heat generation and reaction rates are constant for all types (dimension) of models.

3.1.1.1 Positive solvent reaction

Q_{pe} is the heat generated at the positive electrode, and because the electrode is oxidised, as it decomposes oxygen is released, which then combines with the electrolyte to produce heat. Overall, a significant amount of heat is generated from the process, making it highly exothermic. This reaction can be described by the formulation:

$$\frac{d\alpha}{dt} = \alpha(1-\alpha).A_{pe}.\exp\left(-\frac{E_{pe}}{k_b T}\right) \quad \text{.....(4)}$$

Where α is the degree of conversion at the positive electrode, k_b is the Boltzmann constant, A_{pe} is the frequency factor, E_{pe} is the activation energy and T is the instantaneous temperature. The heat generation at the positive electrode can be given as:

$$Q_{pe}=m_{pe}*H_{pe}*\frac{d\alpha}{dt} \quad \text{..... (5)}$$

3.1.1.2 Negative solvent reaction

The heat generated at the negative electrode is Q_{ne}. When the temperature hits around 120°C, heat released by the SEI decomposition reaction starts the reaction at the negative electrode, and it can be stated in the Arrhenius form as explained in the literature [5].

$$\frac{dx_{ne}}{dt} = -x_{ne}.A_{ne}.\exp\left(\frac{E_{ne}}{k_b T}\right).\exp\left(-\frac{z}{z_0}\right) \quad \text{.....(6)}$$

Where, x_{ne} is dimensionless representation of concentration of Li-ion content which is intercalated between the layers of graphite at the negative electrode, A_{ne} is the frequency factor, E_{ne} is the activation energy of the reaction, k_b is the Boltzmann constant and T is the instantaneous temperature. Additionally, there is a term z that

represents the SEI layer thickness in a dimensionless manner and whose formulation is represented by the following Arrhenius equation.

$$\frac{dz}{dt} = x_{ne}.A_{ne}.\exp\left(\frac{E_{ne}}{k_b T}\right).\exp\left(-\frac{z}{z_0}\right) \quad \ldots\ldots\ldots\ldots\ldots\ldots (7)$$

Now, to get the heat generation we have to multiply the reaction rate with mass of Li content and the enthalpy associated with it.

$$Q_{pe} = - m_{ne} * H_{ne} * \frac{dx_{ne}}{dt} \quad \ldots\ldots\ldots\ldots\ldots\ldots\ldots\ldots (8)$$

3.1.1.3 SEI decomposition reaction

The SEI layer is created through the reduction of the electrolyte and graphite. Long-term cycling stability of LIB is caused by SEI. However, it was observed that SEI layer decomposition starts to occur at increasing temperatures, which is the first step towards the development of TR of LIB. A subsequent cathode reaction is started by heat released as a result of anode reactions, which are set off by the beginning of SEI layer disintegration. As a result, while SEI layer contributes to stability, LIB is prone to TR because of SEI layer's instability at higher temperatures. Q_{sei}, then, is the heat generated by the breakdown of the metastable SEI layer. The majority of SEI's decomposition takes place between 90°C and 120°C, and it can be expressed in the form described in the literature [5].

$$\frac{dx_{sei}}{dt} = -x_{sei}.A_{sei}.\exp\left(-\frac{E_{sei}}{k_b T}\right) \quad \ldots\ldots\ldots\ldots\ldots\ldots (9)$$

Where x_{sei} is the dimensionless representation of concentration of the Li content in the metastable SEI layer, A_{sei} is the frequency factor, E_{sei} is the activation energy of the reaction, k_b Boltzmann constant and T is the instantaneous temperature. Now in order to get the heat generation we will have to multiply the reaction rate with mass of the Li content in SEI layer and the enthalpy associated with it. Therefore,

$$Q_{sei} = -m_{sei}.H_{sei}.\frac{dx_{sei}}{dt} \quad \ldots\ldots\ldots\ldots\ldots\ldots\ldots\ldots (10)$$

3.1.1.4 Heat generation due to short circuit

As a result of the initial charge present in LIB and the subsequent short circuit, electrical energy is transformed into heat energy. As it is well known, LIB's charge content fluctuates. State of charge (SoC), is a word that is used to describe the variation in charge. Therefore, SoC is the way of representing the charge of a LIB. SoC is defined as the ratio of the LIB's full charge content to its instantaneous charge content. As a result, a LIB's SOC is 100 % when it is completely charged, and it is 0% when it is entirely discharged. Coman et al. [5] simplified the variation of SoC and put it in Arrhenius form to make the calculations easier. As a result, the Arrhenius version of SoC is represented by:

$$\frac{d_{SOC}}{dt} = -ISC_{cond}.SOC.A_{SOC}.exp\left(-\frac{E_{SOC}}{k_b T}\right) \quad \text{..... (11)}$$

Where ISC_{cond} = 0 if LIB temperature <57°C

ISC_{cond} = 1 if LIB temperature >=57ºC

In the above equation, we used a term ISC_{cond}. It makes sure that only when the wax of the internal short circuit device (ISCD) melts will the internal short circuit (ISC) and heat generation caused by the ISC be initiated. Because wax melts at 57°C, a temperature condition of 57° is applied.

Heat generation due the state of charge is given as;

$$Q_{SOC} = -H_{SOC} * \frac{d_{SOC}}{dt} \quad \text{..... (12)}$$

We can determine H_{SOC} by using our knowledge of physics. But in order to account for the venting impact as mentioned by Coman et al. [5], we will multiply an additional efficiency term η. Therefore,

$$H_{SOC} = V.C.\eta.3600 \quad \text{..... (13)}$$

Values of all the constants used in all the above equations are given in the Table 2.

3.1.2 Table 2: List of constants used for solving the equation

Parameter	Value	Unit	Source
m_{ne}	8.1 E-3	kg	Coman et al [5]
m_{pe}	18.3 E-3	kg	Coman et al [5]
H_{ne}	1714000	J kg^{-1}	Coman et al [5]
H_{pe}	314000	J kg^{-1}	Coman et al [5]
H_{sei}	257000	J kg^{-1}	Coman et al [5]
H_{SOC}	10160.64	J kg^{-1}	Coman et al [5]
A_{ne}	2.5 E13	**s^{-1}**	Kim et al [2]
A_{SOC}	3.37 E12	s^{-1}	Kim et al [2]
A_{sei}	1.67 E15	s^{-1}	Kim et al [2]
A_{pe}	6.67 E11	s^{-1}	Kim et al [2]
E_{ne}	2.24 E-19	J	Coman et al [5]
E_{sei}	2.24 E-19	J	Coman et al [5]
E_{SOC}	1.58 E-19	J	Coman et al [5]
E_{pe}	2.03 E-19	J	Coman et al [5]
k_b	1.38 E-23	-	Boltzmann constant
V_{cell}	1.66 E-5	m^3	Calculated
$x_{sei,0}$	0.15	-	Coman et al [5]
$x_{ne,0}$	0.75	-	Coman et al [5]
$x_{pe,0}$	0.04	-	Coman et al [5]
$x_{z,0}$	0.033	-	Coman et al [5]
$x_{SOC,0}$	1	-	Coman et al [5]
ρ_{jr}	2580	kg m^{-3}	Coman et al [5]
$C_{p,jr}$	830	J kg^{-1} K^{-1}	Coman et al [5]
K_{jr}	3.4	W m^{-1} K^{-1}	Hatchard et al [1]
r_{cell}	0.009	m	Hatchard et al [1]

Q_{flux}	22700	W m^{-3}	Fitted
h_{conv}	7.17	W m^{-2} K^{-1}	Coman et al [5]
ε	0.8	-	Coman et al [5]
V	4.2	Volt	Coman et al [5]
C	2.4	Ah	Coman et al [5]

3.2 Numerical modelling of PCM

For PCM simulation, the **enthalpy-porosity technique** [35] was used. The solid-liquid interface is not explicitly tracked by this method. The mushy zone is instead treated as porous, with the porosity being equal to the melt fraction (or volume fraction) associated with each cell in the computational domain. The phase shift material transitions from the solid to liquid phase during melting through a region known as the **mushy zone**. A mushy zone is a semi-solid region considered in between the solid and liquid phases. The cell volume percentage that is in liquid form is indicated by the melt fraction. The "enthalpy-porosity approach," which is a significant modification of the enthalpy formulation, is also connected to the liquid fraction, f. The latter is predicated on an apparent resemblance between fluid flow through a porous medium and the partially liquid material in the mushy zone. Evidently, it is used when a liquid medium is handled appropriately and allowed to flow. The main benefit of this method is that it enables variable transformations to be avoided while solving the coupled momentum and energy equations on a fixed grid. The following relevant assumptions have been made to maintain the complexity level at a manageable level.

3.2.1 Assumptions

- The melting PCM behaves like a Newtonian fluid.
- Except for the body force term, the flow is two-dimensional, laminar, and incompressible.
- For the solid and liquid phases, PCM has different properties.
- Both the solid and liquid phases are homogeneous, isotropic, and at thermal equilibrium with the contact.
- Viscous dissipation effects and thermal radiation are negligible.
- The **Boussinesq approximation**, which is given as $\boldsymbol{\rho_l - \rho = \rho_l \beta (T - T_m)}$, where $\boldsymbol{\beta}$ is the coefficient of thermal expansion of PCM, $\mathbf{T_m}$ is the average melting temperature of PCM**.** It provides a good description of the density stratification within the fluid elements.

Due to their dependency on the melt fraction, all of the PCM's thermo-physical properties—density, thermal conductivity, and specific heat capacity—aside from the viscosity—are functions of temperature.

3.2.2 Governing Equations of PCM

The time-dependent continuity, momentum, and energy equations are expressed as follows and, under the above-mentioned presumptions, regulate the coupled velocity and temperature fields. The PCM system's governing conservation equations are-

Continuity equation:

$$\frac{\partial \rho}{\partial t} + \nabla.(\rho V) = 0 \quad \text{..... (14)}$$

Momentum equation:

$$\frac{\partial (\rho V)}{\partial t} + \nabla.(\rho V) = -\nabla p + \mu \nabla^2 V + \rho g + S_m \quad \text{..... (15)}$$

Energy equation:

$$\frac{\partial(\rho H)}{\partial t} + \nabla.(\rho V H) = k\nabla^2 T + S_h \ldots\ldots\ldots\ldots\ldots\ldots (16)$$

Where ρ is the density, V is the velocity vector, p is the pressure, T is the temperature, S_m is the momentum source term, H is the specific enthalpy, k is the thermal conductivity, μ is the dynamic viscosity and g is the gravitational acceleration. The sum of sensible enthalpy (h) and latent enthalpy (ΔH) is known as the specific enthalpy (H).

$$\mathbf{H = h + \Delta H} \ldots\ldots\ldots\ldots\ldots\ldots (17)$$

Where the expression for the sensible enthalpy is-

$$\mathbf{h = h_{ref} + \int_{T_{ref}}^{T} C_p \; dT} \ldots\ldots\ldots\ldots (18)$$

Where, h_{ref} is reference enthalpy at the reference temperature $T_{ref,}$ C_p is the specific heat. Latent heat content can range from 0 (for a solid) to 1 (for a liquid).

$$\Delta H = \beta L_f \ldots\ldots\ldots\ldots\ldots\ldots (19)$$

Here, L_f is the latent heat of fusion and β is the liquid fraction defined as follows:

$$\beta = \begin{cases} 0 \; if \; T < T_s \\ \frac{T - T_s}{T_l - T_s} \; if \; T_s < T < T_l \\ 1 \; if \; T > T_l \end{cases} \ldots\ldots\ldots\ldots\ldots\ldots (20)$$

Here T_s is the solidus temperature and T_l is the liquidus temperature. The energy source term S_h used in equation (14) is given as:

$$\mathbf{S_h} = \frac{\partial(\rho \Delta H)}{\partial t} + \nabla.(\rho V \Delta H) \ldots\ldots\ldots\ldots\ldots (21)$$

The momentum source term S_m used in equation (13) describes flow in a porous medium can be represented as a function of melt fraction as follows.

$$\mathbf{S_m = A(\beta)\, V} \quad \ldots\ldots\ldots\ldots\ldots\ldots \quad (22)$$

Brent et al [36] defined A(β) as the porosity function. The source term, which was used to describe the flow in the porous medium in the momentum equation, has to be zero in the liquid phase to allow for free motion but it has to be large in the solid phase to force the velocity values to near zero values [37]. The Carman-Kozeny equation, which is deduced from the Darcy law for fluid flow in porous media, is most frequently used in a modified form:

$$\mathbf{A(\beta)} = \frac{\boldsymbol{A_{mush}(1-\beta^2)}}{\boldsymbol{\beta^3+\varepsilon}} \quad \ldots\ldots\ldots\ldots\ldots\ldots \quad (23)$$

where A_{mush} is the mushy zone constant, which indicates how quickly the fluid velocity approaches zero as it solidifies, and ε is a tiny computational constant employed to prevent zero in the denominator (in this study $\varepsilon = 0.001$).

The velocity switch-off in solid PCM is accounted for in the aforementioned formula (21) by the function A(β). When the entire PCM melts ($T > T_l$), the source term (S_m) in the momentum equation approaches 0 and the melt fraction $\beta \rightarrow 1$, approaching the general momentum conservation equation that applies to a Newtonian fluid flow. However, the entire PCM is solid and hence $\beta \rightarrow 0$ when the temperature of the PCM is lower than the solidus temperature ($T < T_s$). Since the flow velocity is almost nil in this situation, the source term's contributions are quite small. As a result, the source term only makes a significant contribution to the melting process in the mushy zone (i.e., within melting regime).

The PCM melting properties and heat transport in this regime are mostly regulated by the mushy zone parameter A_{mush}. The location of the solid-liquid melting interface and how it moves throughout the melting process are greatly influenced by the values of this parameter, which depends on the geometry of the PCM. The solid-liquid interface can be accurately predicted by sufficiently large values of A_{mush}, which suppress the flow in the PCM's solid regions. Low values of A_{mush} produce inaccurate

predictions when defining the moving solid-liquid interface, whereas high levels of A_{mush} produce oscillating outcomes. As an alternative, extremely high values of A_{mush} imply a greater volume of the PCM in the mushy area, which is primarily static. This underestimates how the PCM actually behaves in natural convection, whereas very low values of A_{mush} overestimate the amount of melting. Therefore, it is essential to choose the A_{mush} parameter with care while planning the numerical modelling of the melting process. In most computations, values between 10^4 and 10^7 kg/m^{3}s are advised [33].

3.3 PCM cooling under constant heat generation

In this case we have taken three scenarios. First, we have tried to see the effect of PCM by taking two cases as with PCM cooling and without PCM cooling. Second, we have seen how the variations of convective heat transfer co-efficient (h) effects the battery heat generation and melting time of the PCM. Lastly, we have tried to capture the intermittent operation of PCM by observing the melting and solidification process. For all three processes we have taken a 18650 LIB with a PCM covering it having a thickness of 9 mm.

3.3.1 Geometry and meshing

Figure 6: Geometry and meshing for the study

Figure 6 shows the geometry files and mesh files for the PCM and battery configuration. Here the diameter of the battery is taken 18 mm and surrounding it there was a PCM with 9mm thickness. Lauric acid was used as the PCM here. The geometry was created with the help of ANSYS design modeller.

ANSYS meshing tool was used to discretise the geometry. Total 29317 nodes and 28778 elements were used to perform this simulation. Average orthogonal quality was 0.98 and average skewness was 0.08 which depicts that the meshing is of good quality. Face sizing was used for the whole domain. The element size of meshing was 0.2 mm.

3.3.2 Heat generation calculation

Battery operation typically involves a variable charging and discharging cycle. Heat generation thus varies from time to time as well as from operating cycle to operating cycle. To begin with, we must therefore understand the heat generating range for the BTMS parametric investigation.

Here we have taken a 18650 LIB with 1C heat generation. The battery capacity is 2.4 Ah.

Volume (v) of the battery = $\frac{\pi}{4} d^2 l = \frac{\pi}{4} . (0.18)^2 . 0.065$ m^3 = 1.65 x 10^{-5} m^3

We know, Current = Battery capacity x C – Rate = 2.4 x 1 = 2.4 amp

Heat Input = 2.4 amp x 4.2 Volt = 10.08 W

Volumetric heat generation rate = $\frac{10.08}{1.65\ X\ 10^{-5}}$ W/m^3 = 607228.915 W/m^3

3.3.3 Boundary conditions

Here, in this case we have assumed that the battery is vertically placed. So, gravity is not taken into consideration in this case. The heat generation is taken as the calculated value above. Other than that all other settings are same as we will be discussing at the PCM cooling set-up methodology in the next section.

For with and without PCM cooling study we have taken two geometry one having only battery exposed to h = 20 W/m^2-K, T = 300K and another one with same h and T value but with PCM on it. The purpose of this study is to see the effectiveness of PCM.

For the next study we have taken different h values to see its influence on the battery temperature and melting time. We took three values of h for this study, they are h = 20, 100, 200 W/m^2-K and T = 300K was taken same for all three studies.

For the last one we have used two different boundary conditions for melting and solidification. For melting we took h = 20 W/m^2-K, T = 300 and for solidification h = 400 W/m^2-K, T = 280 K to propose a model where we can almost equate the melting and solidification time. During melting the battery heat generation was set to the above value and for the solidification heat generation was set to 0.

3.4 Physical model for air and PCM cooling

The computational domain and meshing used for this numerical simulation of battery-cell heat transfer using air cooling and PCM cooling is shown in the **figure 7.** The module shown contains one 18650 $LiCoO_2$ LIB. The battery has a diameter of 18 mm and height of 65 mm but here we are performing a 2-D numerical simulation that's why it is shown as circular. This same geometry is used for both air cooling and PCM cooling.

3.4.1 Geometry and meshing for air and PCM cooling

As both the setups are same for the air and PCM cooling their geometry and meshing was also the same. The geometry along with the dimensions and mesh files that are used for this simulation is shown in **figure 7**. The geometry was created with the help of ANSYS design modeller.

A total 8922 number of elements and 5667 number of nodes were used for this study. ANSYS meshing tool was used to discretise the geometry. All triangles elements were used in the whole domain. Face meshing was used for the battery, rectangular area which was used for air domain/PCM domain. Edge sizing was given to the battery and the air/PCM interface to refine the mesh a little bit. This is because near the battery wall zone or interface zone there is solid-fluid contact or interaction is happening. Due to conjugate heat transfer a boundary layer is formed over there. So, to capture the heat transfer effect more accurately we have to create a mesh interface zone there and finer mesh needs to be created to capture the rapid movement of properties at the interface. The skewness and orthogonal quality of the meshing was within the excellent range.

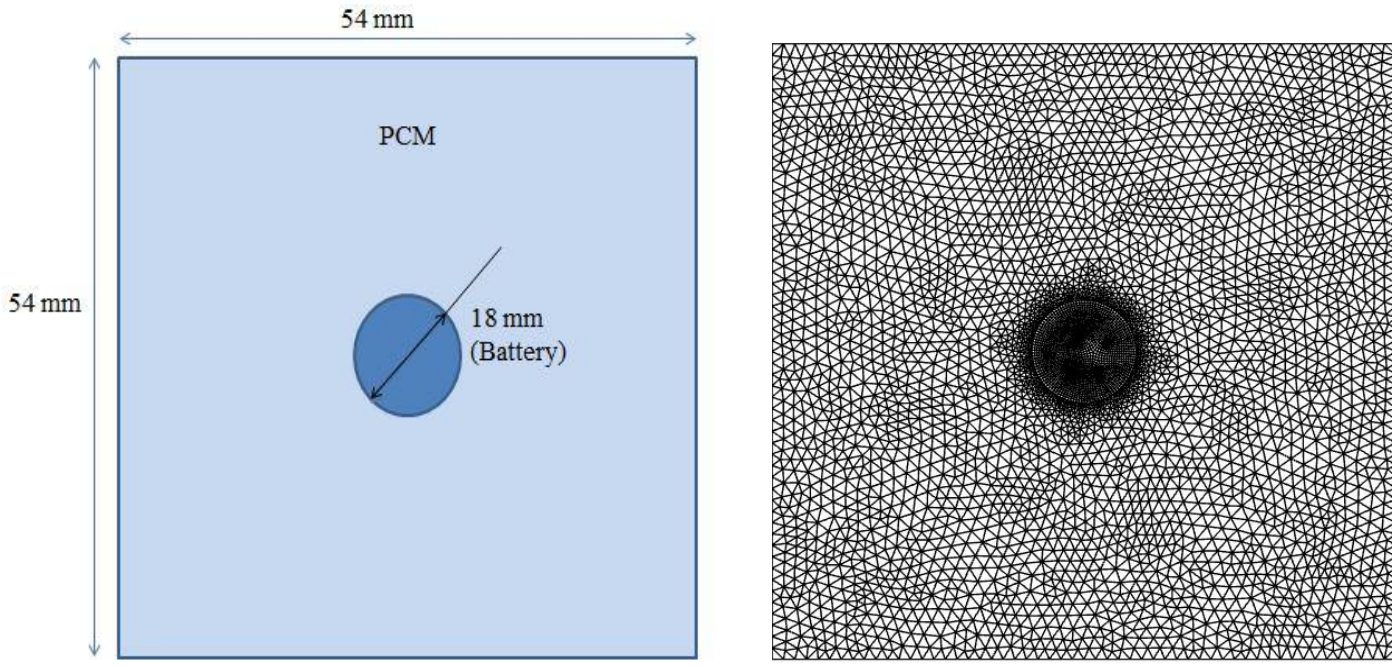

Figure 7: Geometry and meshing of physical model

3.4.2 Numerical modelling for Air cooling

In this case we are assuming that the battery is placed horizontally so that the gravity is acting in the negative y direction of the co-ordinate system. A pressure-based transient solver was used with gravity of -9.81 m/s^2. Energy and standard k-epsilon model was activated. The properties of the battery and air are listed in **table 3** and **table 4** respectively.

3.4.2.1 Table 3: Properties of $LICoO_2$ battery

Sl no	Parameters	Value
1	Density (kg/m^3)	2580
2	Specific heat (J/kg-k)	830
3	Thermal conductivity (W/m-K)	3.4

3.4.2.2 Table 4: Properties of air

Sl no	Parameters	Value
1	Density (kg/m^3)	1.225
2	Specific heat (J/kg-K)	1006.43
3	Thermal conductivity (W/m-K)	0.0242
4	Viscosity (kg/m-s)	1.78 E-5

For the heat generation inside the battery a user defined function (UDF) was used. This will be discussed later in the battery modelling section. Same process of battery modelling is followed as the validation battery modelling except here the ISC part was removed from the UDF.

At the inlet a velocity of 1m/s was given and at the outlet pressure-outlet boundary condition was used. At the top and the bottom wall a convective boundary condition (h=20 W/m^2-K, T = 300 K) was used. Where h is the convective heat transfer co-efficient and T is the free stream temperature. Solution methods, under-relaxation factors and residuals were set as default. The whole domain was initialised to 300K and the user scalars used are from the battery validation literature [5]. Time step size of 0.001 seconds and maximum iteration of 40 was used.

3.4.3 Numerical modelling for PCM cooling

In this case of simulation gravity plays a significant role. The density difference between the fluid elements is described by **Boussinesq approximation.** The Boussinesq approximation is employed in the study of buoyancy-driven flow in fluid dynamics (also known as natural convection). It doesn't take into account density variations unless they are expressed in terms multiplied by g (Gravitational acceleration). The Boussinesq approximation's main idea is that while there is a small difference in inertia, gravity is powerful enough to make the specific weight noticeable. When a fluid's temperature varies from one location to another, causing a flow of fluid and heat transfer, the Boussinesq approximation is used.

In the case of PCM simulation, along with the energy and viscous model, the solidification and melting model was used. **Mushy zone parameter value** (A_{mush}) was taken as constant (= 2 x 10^5) which is taken same as the PCM paper work done by Fadl et al [33], which was validated. The details of mushy zone parameter are discussed in the Computational set-up of PCM section. In this case the PCM domain is taken as fluid medium. The properties of the PCM (in this case Lauric acid) are listed in the **table 5** below.

3.4.3.1 Table 5: Thermo-physical properties of the lauric acid as the PCM [33]

Sl no	Property	Solid	Liquid
1	Liquidus temperature, T_l (K)	-	321.35
2	Solidus temperature, T_s (K)	316.65	-
3	Melting temperature, T_m (K)	319	
4	Density, ρ (kg/m^3)	940	885
5	Specific heat, C_p (J/kg-K)	2180	2390
6	Thermal conductivity, k (W/m-K)	0.16	0.14
7	Viscosity, μ (kg/m-s)	-	0.008
8	Thermal expansion co-efficient, β (1/K)	0.0008	
9	Latent heat of fusion, L_f (J/kg)	187210	-

Nearly 4.7 K (=2ΔT) is the transition temperature range (or melting range) taken into account in this work, where (T_m - ΔT) is thought of as the "solidus" temperature and (T_m + ΔT) as the "liquidus" temperature.

The battery property was same as **table 3**. The UDF and the cell zone conditions were same as the air flow run. Unlike the air flow simulation, boundary conditions were imposed in all the four edges (walls) of the square cavity. At the walls convective boundary condition (h=20 W/m^2-K, T = 300 K) was used.

Pressure-velocity coupling was accomplished using the semi-implicit approach for the pressure linked equations **(SIMPLE)**, and the pressure terms' spatial discretization and interpolation were accomplished using the **PRESTO** (Pressure Staggering Option) scheme [34]. The advection component was discretized using a **second order upwind** method, the diffusion term was discretized using **central differencing (First order upwind)**, and the transient term was discretized using a **second order implicit** discretization scheme. The under-relaxation factors employed were 1, 0.7, 0.3, 1, and 0.9 for density, momentum, pressure correction, thermal energy, and melt fraction, respectively.

In order to meet the convergence conditions of 10^{-3} for the velocity components and continuity and 10^{-6} for the energy equations, the maximum number of iterations for each time step was set at 40. Volume average liquid fraction of the PCM zone were plotted with against time using the volume monitor and the facet average value of interior battery was calculated using surface monitor. The solution was initialised at 300 K with the user scalars with a time step size of 0.001 seconds. The air domain and the battery domain were patched at 300 K.

3.5 Grid independence study

The results of simulations will be more accurate and realistic if the computational model meshing is carried out in a highly precise and detailed manner. Convergence of iterations, simulation speed, and accuracy are all significantly influenced by the meshing process. Since meshing takes up a lot of our time while getting simulation results, we need speed up the refinement process so that the outcome of our simulations is independent of the number of elements and grid size.

In order to study grid independence we took one meshing with 8900 elements and another one with 17800 elements which is twice of the first one. After performing the simulations we observed almost similar results. So we can say that the grid we chose is the optimum one.

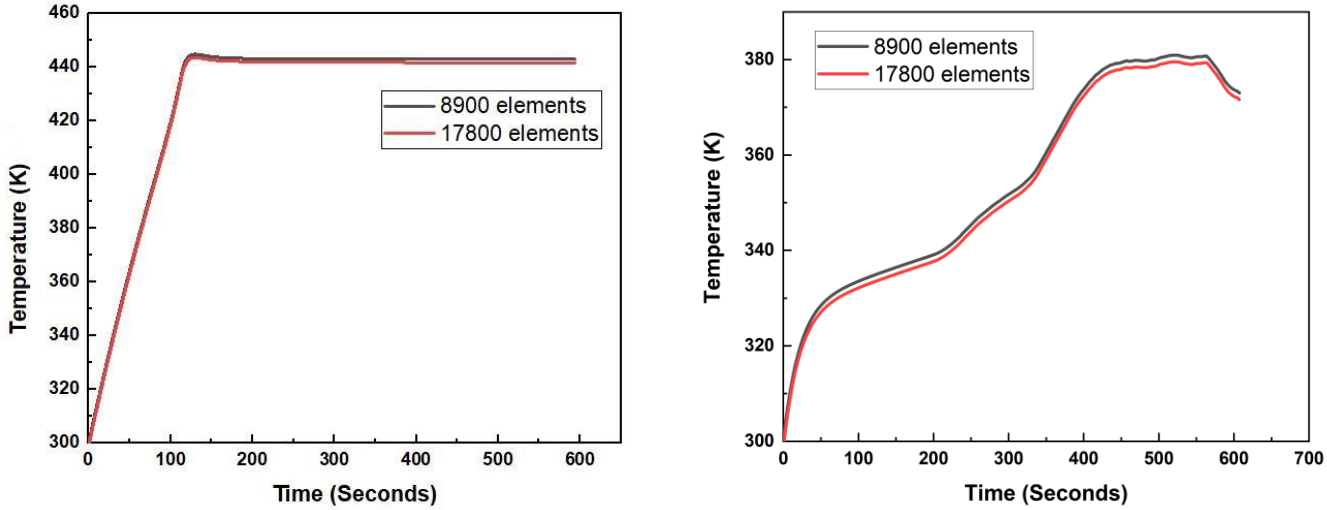

Figure 8: Grid independence study of air and PCM cooling.

3.6 Battery validation

It is possible to use a 2-D or 3-D LIB model to analyse TR in a single LIB. Each type has advantages and disadvantages of its own. Since 18650 Li-ion batteries can be regarded as a lumped body because their Biot number is less than 0.1, Hatchard et al. [1] propose that a 1-D model of LIB is feasible. In many governing equations, a single temperature can therefore be employed for calculating purposes. Thus, 2-D models take less time to compute, but we are unable to see the effects of local heating or cooling, as well as the spatial fluctuation of temperature and other parameters. So, we run 3-D simulation to acquire a clearer image of real-world circumstances, but it takes more time overall. We shall see the 2-D modelling in this section. For this reason, Kim et al [2] expanded the work of Hatchard et al [1] from 1-D model to 3-D model. It was discovered that the exothermic reaction propagates initially in such a way that it forms a hollow cylinder-like reaction zone at radius and zone travels from the outer radius towards the centre. This was done by converting a 1-D model to a 3-D model in order to understand the effect of local hot spots on thermal abuse behaviour of LIB. So, we run 3-D simulation to acquire a clearer image of real-world circumstances, but it takes more time overall.

The next thought after choosing the model is how to get our LIB to a point where TR happens to complete the process of testing the LIB through numerical investigation. There are several ways to do it, including ISC, nail penetration, and oven heating. In reality, before batteries are put on the market, their safety is tested using oven heating, nail penetration, and ISCs. We will employ the ISC employing ISCD technique employed by Keyser et al. [38] in the current investigation. The melting of the separator or the presence of the conducting materials in the LIB can cause the anode and cathode to come into contact, which can result in an ISC. An ISCD was created by Keyser et al. [38] and is placed into LIB to cause a short circuit. Wax is present in ISCD, and when wax reaches its melting point, it melts and causes a short circuit. Wax was melted in the experimental investigation using a heater. Although LIB is not linked to any electrical circuits during the experiment, it has an initial state of charge (SoC). The initial temperature of LIB is 293K, which is the same as the outside

temperature. When the heater is turned on, heat flux is given into the LIB through conduction. Wax melts (at roughly 57°C) as a result of heating, causing an internal short circuit. It is assumed that electrical energy is transformed to thermal energy because of ISC. This heating causes the LIB's different components, including the Solid Electrolytic Interface (SEI), Positive Electrode (PE), Negative Electrode (NE), and Electrolyte (E), to break down quickly and generate a lot of internal heat. TR of LIB results from an imbalance between the rate of heat produced and the heat transferred outside to ambient.

The Biot number for LIBs is less than 0.1 when calculated. As a result, we can consider LIB to be a single mass and use that temperature wherever it is needed in calculations. Additionally, it helped us gain understanding of how various constants and terms related to heat transfer coefficients affect temperature and response rate.

3.6.1 Numerical modelling

A user defined function (UDF) based on the value given in table 2 and the different abuse condition reactions based on Arrhenius formulations was written in C programming language to simulate the TR in LIB for the 2-D modelling approach. The equations are described in the literature [5]. The code was interpreted in ANSYS FLUENT 16 software. An 18650 LIB was used for the simulation. Total 6998 number of elements and 7129 number of nodes were used. A pressure-based solver along with transient formulation was used. The battery property values are mentioned in the table 2, which are taken from Coman et al [5]. Five user defined scalars (UDS) were used for negative electrode, positive electrode, SEI layer, State of charge and degree of conversion. At the battery wall mixed thermal boundary conditions were applied with convective heat transfer co-efficient and emissivity as described in table 2 and external radiation temperature and free stream temperature as 293K. The solution was initialised at 293K and five user scalars value was fitted same as listed in table 2. The solution methods, under relaxation factors and residuals were set as default configuration. A time step size of 0.001s and 40 maximum iterations were enough to

get a good agreement between our present study and the Coman et al [5] as shown in **figure 9.**

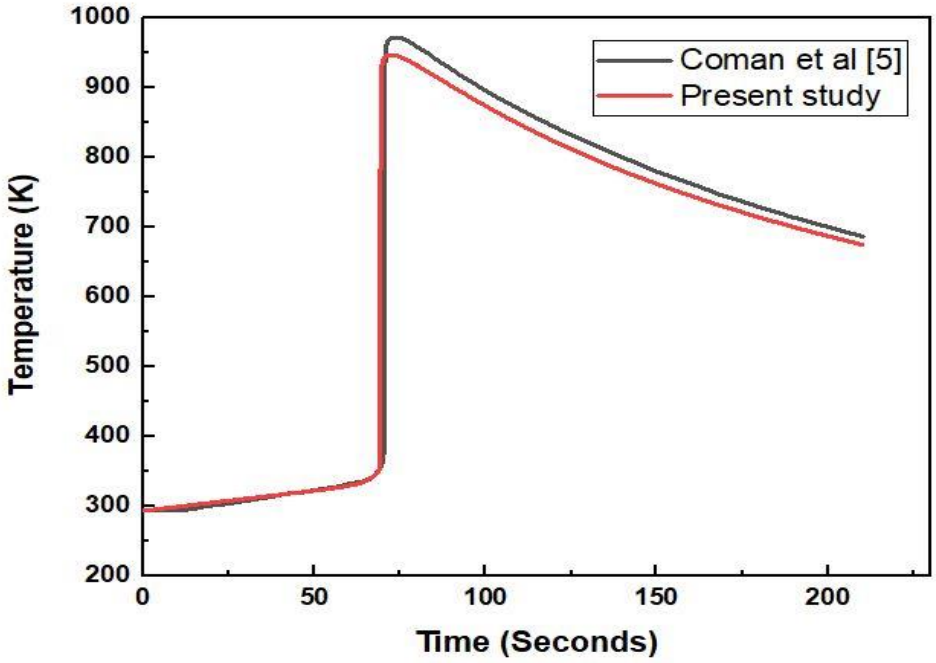

Figure 9: Comparison of Temperature vs. Time graph

3.7 PCM validation

Here we have validated a work by Fadl et al [33] which consists of a container which contains Lauric acid (PCM) in it. They conducted the simulation based on the experimental study done by Kamkari et al [39]. In that study quantification of PCM melting was tracking the shape of melting interface with respect to time. The inside dimension of the container having 0.05 m width, 0.12 m height and 0.12 m depth. Wall of the enclosure was at constant temperature of 70ºC. 0.025 m thick plexiglass sheet was attached with the other three walls of the enclosure having thermal conductivity 0.043 W/m-K.

3.7.1 Numerical modelling

Here, we have validated the specific case of horizontal enclosure with mushy zone parameter (A_{mush}) value of 2 x 10^5. The mesh size and time step size used for the simulation is the optimum one that is used in the study [33] i.e. (50 x120) and 0.2 s. The simulations were executed as 2-D double precision (2ddp) code using the ANSYS FLUENT 16 software. The momentum and continuity equations were solved using the pressure-based coupled technique. In order to forecast natural convection in the PCM during the simulation, the gravity vector was set to - 9.8 m/s2 in the y-direction.

Pressure-velocity coupling was accomplished using the semi-implicit approach for the pressure linked equations **(SIMPLE)**, and the pressure terms' spatial discretization and interpolation were accomplished using the **PRESTO** (Pressure Staggering Option) scheme [34]. The advection component was discretized using a **second order upwind** method, the diffusion term was discretized using **central differencing (First order upwind)**, and the transient term was discretized using a **second order implicit** discretization scheme. The under-relaxation factors employed were 1, 0.7, 0.3, 1, and 0.9 for density, momentum, pressure correction, thermal energy, and melt fraction, respectively.

In order to meet the convergence conditions of 10^{-6} for the velocity components and continuity and 10^{-11} for the energy equations, the maximum number of iterations for each time step was set at 300.

The above computational procedure was used to get a good agreement of our present study with the work by Fadl et al [33]. **Figure 10** shows the comparison between our present works with the literature.

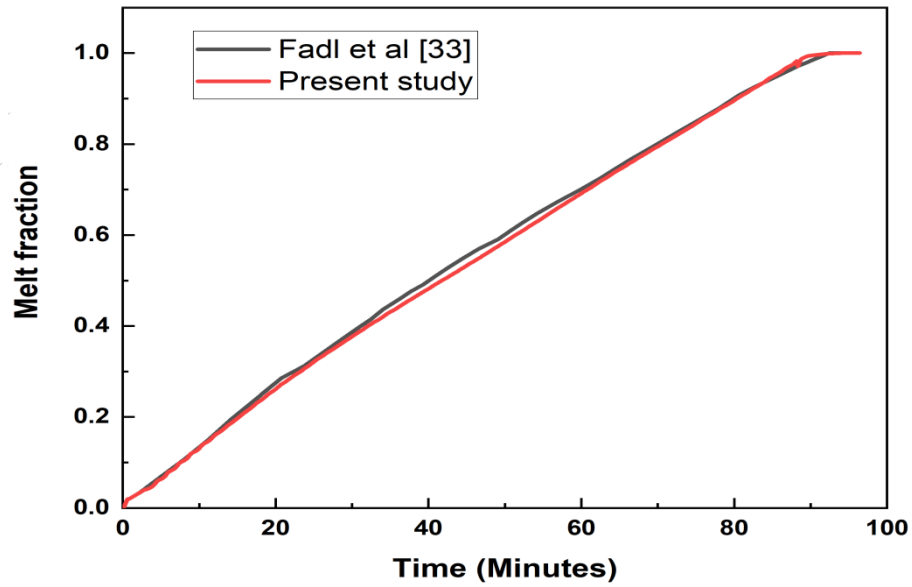

Figure 10: Comparison of Melt fraction vs. Time

Chapter 4

Results and discussion (PCM cooling under constant heat generation)

4.1 Without PCM and with PCM

As we have mentioned earlier that we performed this simulation to know how the temperature inside the battery varies by adding PCM (9 mm thick) to a convective medium. We took h = 20 W/m^2-K and T = 300 K for both the study. **Figure 11** shows the variation of temperature vs. time for these two cases.

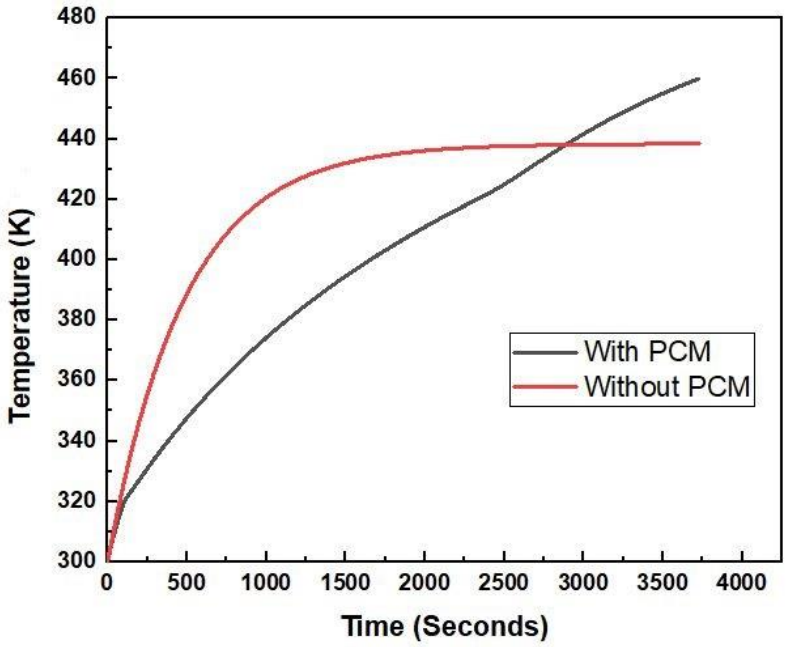

Figure 11: Temperature vs. Time for with and without PCM

As we can see from the graph that without PCM the temperature inside the battery increases at a much faster rate compared to with PCM. Without PCM the temperature reaches a steady value (438 K) after some time. This is because after sometime a situation happens when the heat generation by battery equals the heat taken by convection. The PCM completely melts around 2288 s. Till that time the maximum temperature reached by PCM is lower than the without PCM configuration. Up to that

time the whole PCM domain remains at its phase change temperature i.e. 319 K. If the battery continues to generate heat after the melt fraction becomes 1 (when whole PCM is been melt) then sensible heating of the PCM starts and the temperature increases further than the phase change temperature where it crosses the steady state temperature. We can also explain this by thermal resistance concept-

For without PCM $R_{th} = \frac{1}{h_0 A_0} = \frac{1}{20*2\pi*0.009} = 0.884$ K/W

For with PCM $R_{th} = \frac{1}{h_0 A_1} + \frac{\ln(\frac{r_2}{r_1})}{2*\pi*K*L} = \frac{1}{20*2\pi*0.018} + \frac{\ln(18/9)}{2*\pi*0.14*1} = 1.23$ K/W

Where, A_0 is the outer heat transfer area without PCM which is same as the battery cross sectional area, h_0 is the convective heat transfer co-efficient; A_1 is the outer heat transfer area with PCM, r_2 is the outer radius of PCM, r_1 is the radius of the battery, K is the thermal conductivity of PCM.

We can see than with PCM the thermal resistance is more that's why we can see a more temperature increase in case of PCM than without PCM case for the same heat generation.

4.2 Variation of h with PCM cooling

In our next study we chose three different values of h to see how the influence of h affects the battery's temperature. Here we have taken h = 20, 100, 200 W/m^2-K. Free stream temperature was kept same for all three cases as T = 300 K. **Figure 12** shows the variation of battery temperature along with time at different h values. We can see that initially the temperature remains almost the same despite changing h but after some time we can observe that the graph splits at a point. We have observed as h increases the battery temperature doesn't get affected much but it significantly increases the melting time. So, we can say that increasing the h value doesn't help in cooling of the battery but it helps to increase its runtime for the current configuration.

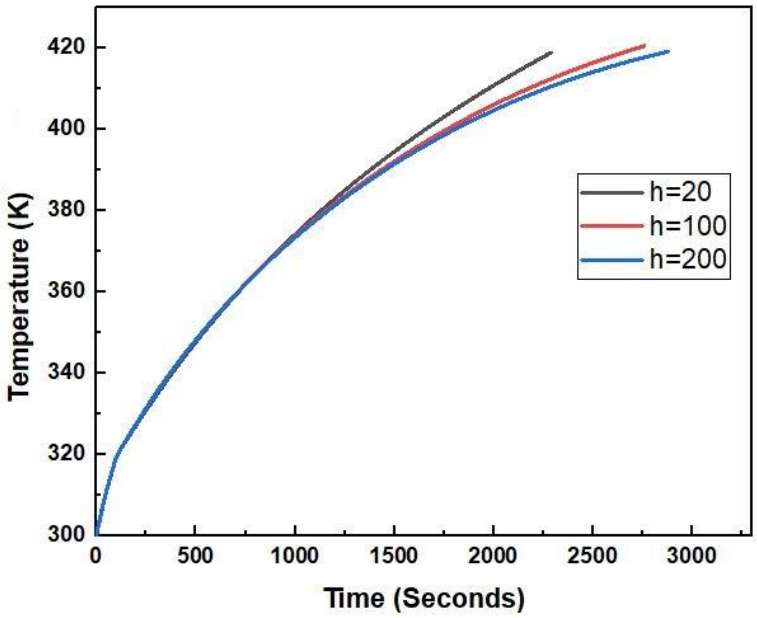

Figure 12: Temperature vs. Time for varying h

4.2.1 Effect on melting time

We can clearly observe from the graph that as the heat transfer co-efficient increases the time required for melting increases. So, we can say that increasing the outside h value can help us to increase the PCM runtime to a significant amount but it doesn't have much effect on the battery temperature. **Figure 13** shows the increase in melting time with increase in h from 20 to 100.

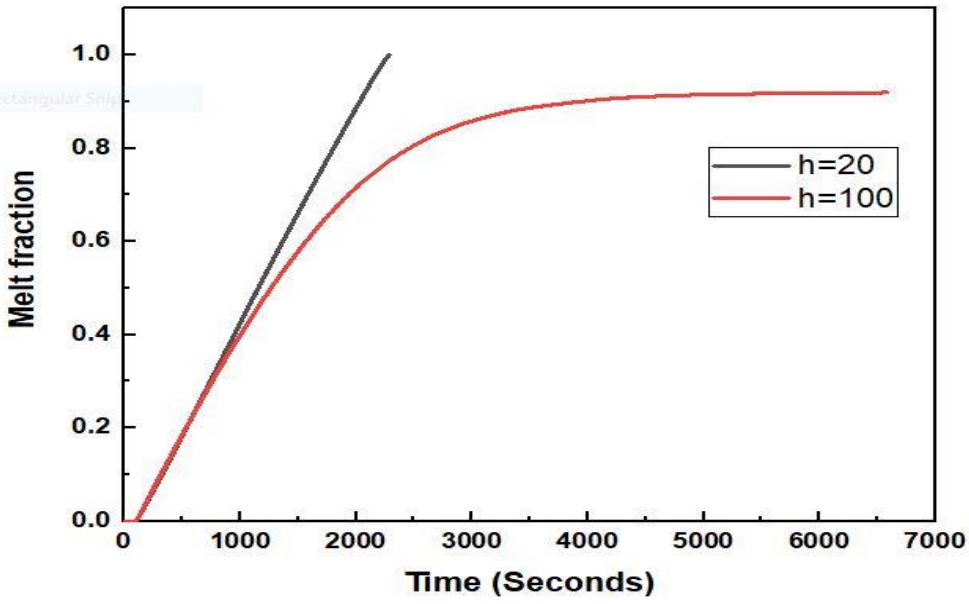

Figure 13: Melt fraction vs. Time for different h

4.3 Melting and solidification

Here in this simulation we have tried to capture the intermittent operation of PCM along with forced convection. Intermittent behaviour of PCM means, the PCM operates in two phases one during melting and another one during solidification. PCM needs energy equal to its latent heat of fusion for phase change (Solid to liquid). During operation, PCM absorbs the transferred heat from the battery and melts.

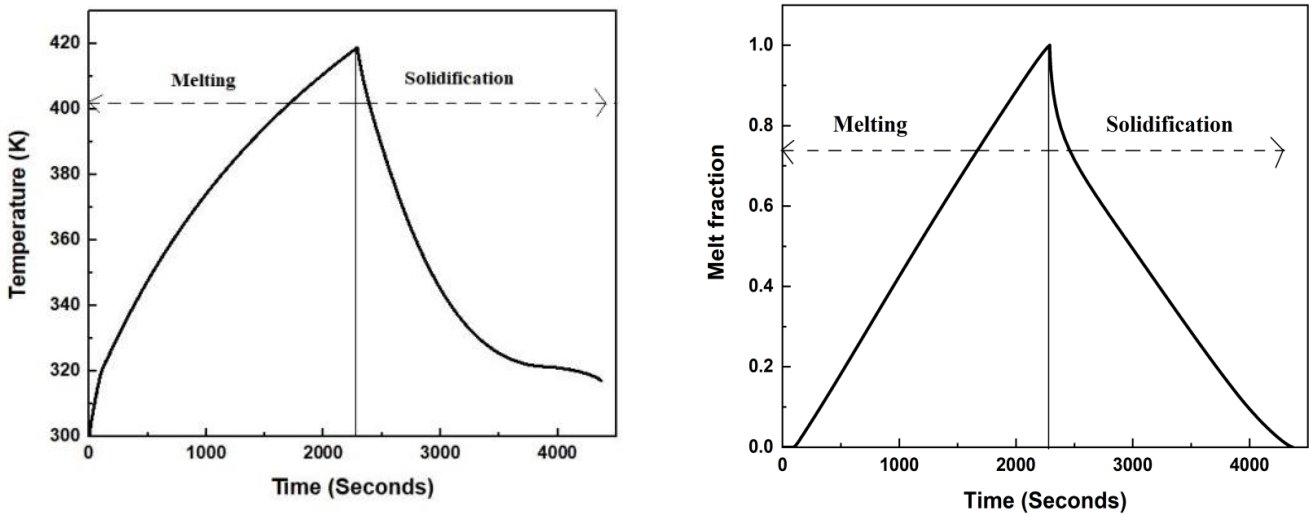

Figure 14: Temperature and Melt fraction variation vs. Time during melting and solidification

During this time it stays at its phase change temperature which is in this case 319 K. Thus it is used as a latent heat storing device. After that the PCM needs to be solidified to bring back to its working state. Here we have used the PCM in the same way first the battery heat generation was set to a constant value as of 3.3.2 and after the melting is done the heat generation was set to 0 and we observed the solidification curve.

Figure 14 shows the temperature and melt fraction variation with respect to time during solidification and melting. As this is the case of 9 mm PCM thickness we took h = 20 W/m^2-K for the melting run and h = 400 W/m^2-K for the solidification run. We can observe from the graph that it took 2288 s for the melting and 2082 seconds for the solidification but the highest facet average temperature reached for the battery is

418 K which exceeds the maximum threshold temperature. Though it can sustain the battery from TR for 250s as up to that time the battery temperature remains under the threshold value. So, to practically use this system we can run the battery at the given C-rate for 250 s. Then we can solidify with the help of external cooling it to reuse the PCM.

If we observe the temperature vs. time curve and the melt fraction vs. time curve we can notice one thing that the slope of temperature line decreases up to the limit when the melt fraction reaches 1. That means the rate of increase of temperature decreases as the melting progresses. This is because the area of the melting regime increases. We can observe the same for the melting rate. Melting propagates fast near the battery and slows down near the end of PCM melting regime. For the solidification we can see fast solidification during the starting but as solidification progresses the rate of solidification decreases. That's why the slope of temperature line also decreases as the solidification happens.

4.3.1 Melt fraction Contours

Figure 15 describes the melt fraction contours at different times for this simulation. We can clearly see that the buoyancy effect is missing here as here we have assumed that the battery is vertically placed so there is no role of gravity in this case. We can also look at the fact that the rate of melting is faster at the initial and it keeps on increasing till the end.

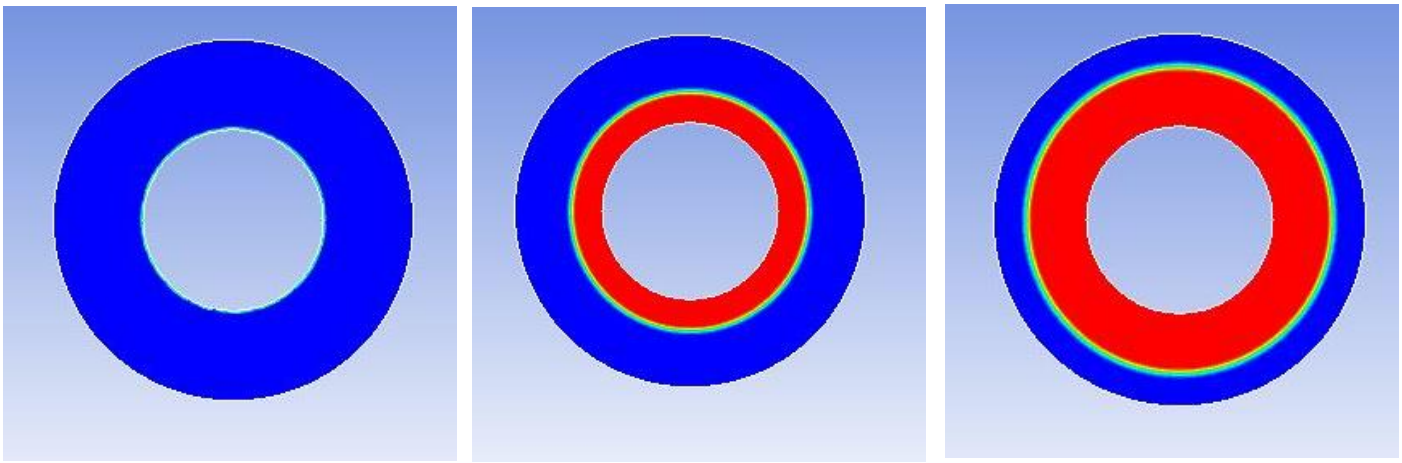

t = 100 s **t = 700 s** **t = 1300 s**

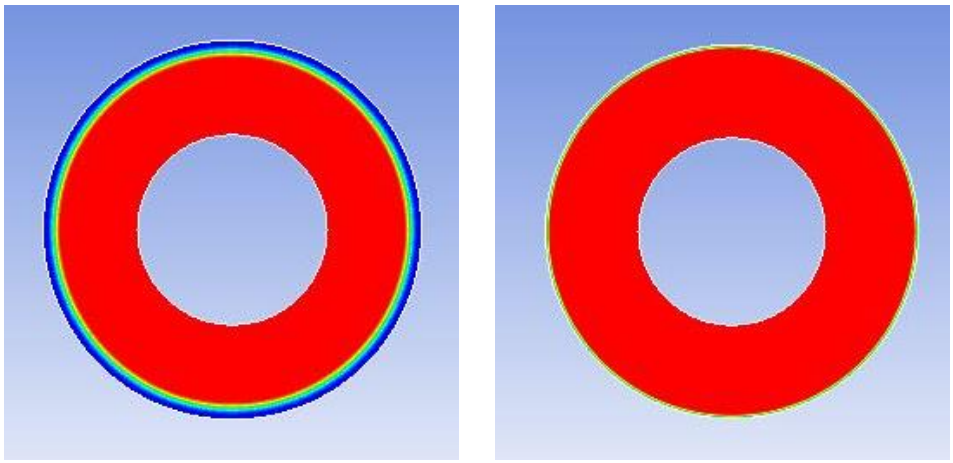

t = 1900 s **t =2290 s**

Figure 15: Melt fraction contours for 9 mm PCM thickness

4.4 Conclusions

From the above results we can conclude that for our scenario, in a convective medium it is better to use PCM as it helps to reduce the temperature but we should not use after the melting completes as it increases the battery temperature significantly.

Also we can say that increasing the heat transfer co-efficient doesn't have much greater impact when we incorporate PCM with convective cooling as it fails to reduce the battery temperature but external cooling can be helpful if we want to increase the runtime of the PCM.

We also have proposed a model where we have incorporated both the melting and solidification of PCM by almost equating the melting and solidification time.

We can also use this study to find the optimum PCM thickness insulation to which a suitable convective heat transfer will enable to perform the battery for a longer period of time. It will also be cost and space effective. From this study we have realised that PCM is very good latent heat storage medium out there but for EV battery cooling applications it should be incorporated with improving methods of PCM. Then it will turn out to be an effective and efficient solution for EV battery cooling applications. Now we will see how it performs under TR conditions.

Chapter 5

Results and discussions (PCM with forced cooling)

5.1 TR result without any cooling

To simply run the UDF, we performed simulation on a single battery with adiabatic condition (heat flux = 0) in its walls to see how the TR happens inside the battery. Unlike the battery validation case here we have ignored the ISC terms. Here, we have taken only the abuse conditions of the battery along with Q_{heater} = 50 W .The facet average value of temperature of inside the battery vs. the time taken (in seconds) is depicted in the **figure 16.**

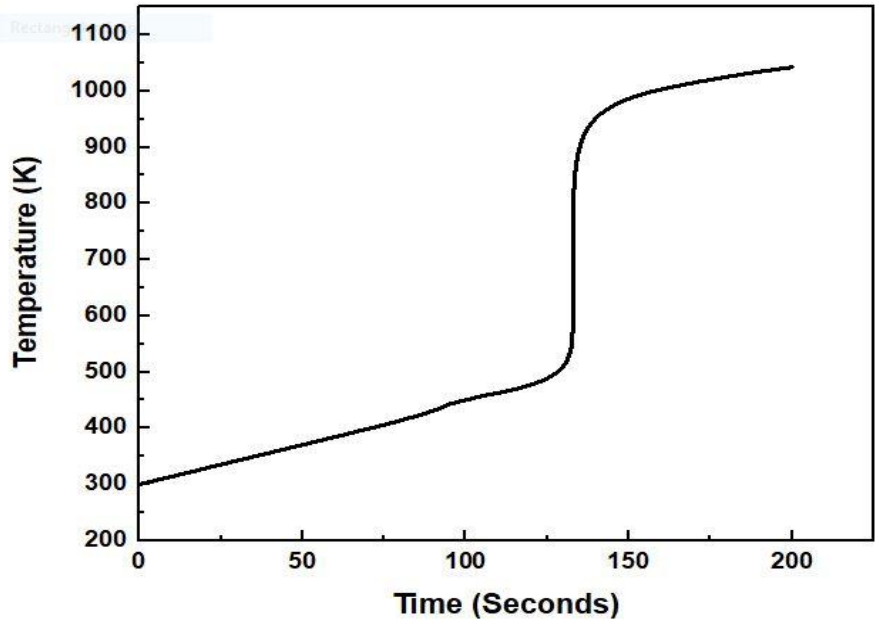

Figure 16: Temperature vs. Time for a single battery

Here we can clearly see the TR happens near about 125 sec where the curve gets an upward deflection. The maximum temperature observed was 1042.429 K at 200 seconds. We can also see that the nature of the graph is similar as Coman et al [5].

5.2 Air cooling results

The air cooling setup and methodology has been discussed earlier. The same UDF is used that is mentioned above is used in the simulation. Air inlet velocity was taken as 1 m/s. The facet average value of temperature of inside the battery vs. the time taken (in seconds) is depicted in the **figure 17.**

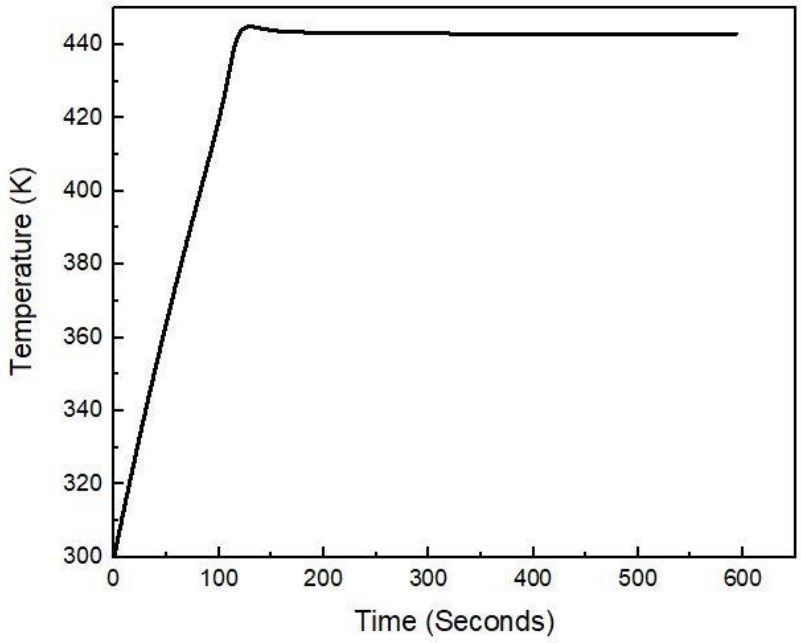

Figure 17: Temperature vs. Time for air cooling

The maximum temperature recorded for air cooling was 444.8626 K which is much higher than the safe operating condition of the battery. So to save the battery for this given configuration, we have to provide more convective cooling by air. But we can see after attaining certain temperature air cooling does not permit to increase the battery's temperature further i.e. it reaches a steady value.

In this case we have to supply more high velocity of air i.e. greater than 1m/s to keep the battery's temperature within the optimum operating range. Now, we will look at how PCM cooling performs under identical working conditions.

5.3 PCM cooling results

Here, in the case of PCM we have observed two data. One is the battery facet average temperature vs. time and the variation of the melt fraction within the square domain vs. time which is shown in the **figure 18** and **figure 19** respectively.

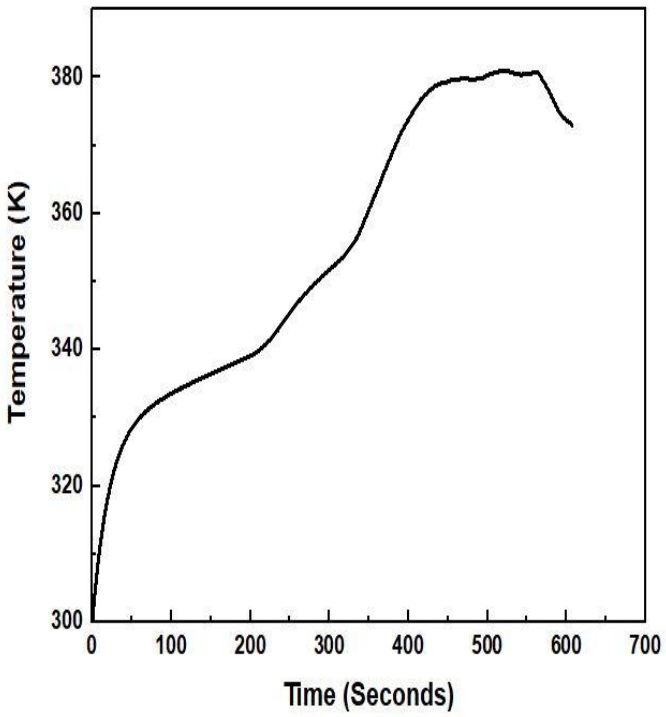

Figure 18: Temperature vs. Time for PCM cooling

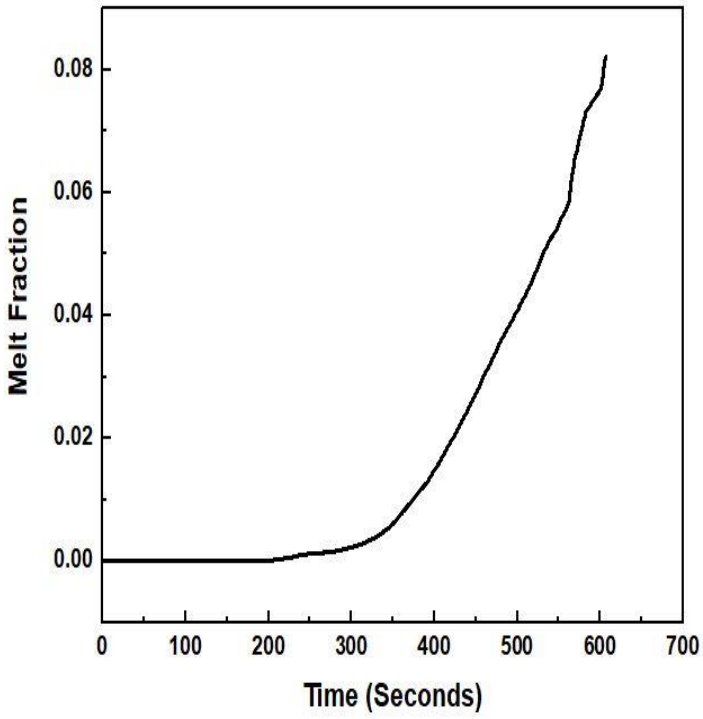

Figure 19: Melt fraction vs. Time for PCM cooling

As we can see that the maximum temperature reached by PCM cooling is much lower than that of in the case for air cooling. The maximum temperature attained by PCM cooling is around 380.93 K.

It needs to be noted that the Q_{heater} value which we have taken for this configuration is quite high i.e. 50W. From the heat generation calculation done at the section 3.2.2 we can see that for a 2.4 Ah capacity battery with 4.2 volt, it needs to operate at 5C rate to generate that much amount of heat. So, it is likely to be possible that the battery will be safe for the both arrangement if the battery is operated in low C rate. Here, in this

configuration we can say that the battery will not be able to perform for a longer period of time but if we can increase the velocity of incoming air and improve the thermal conductivity of the PCM it can provide a longer working time LIBs.

5.4 Air cooling vs. PCM cooling comparison

Figure 20 shows the comparison between the air cooled system vs. PCM cooled system. It clearly depicts the difference between the maximum temperatures attained between the two systems.

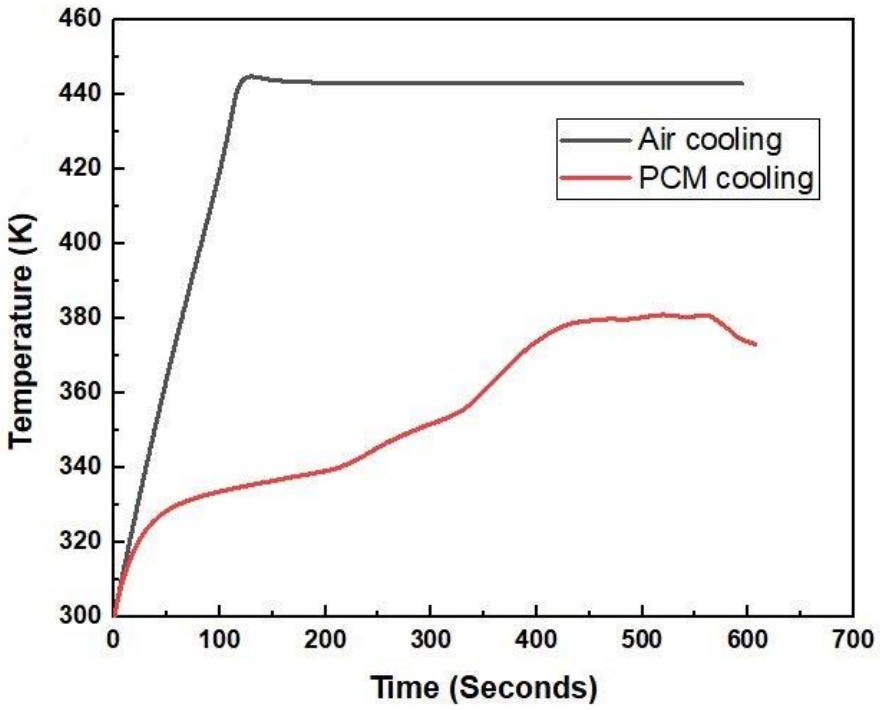

Figure 20: Comparison between air cooling and PCM cooling

Now we will look at the different contours of the PCM cooling method. We will specifically look at the temperature contour and liquid fraction contour to see how the temperature inside the battery and PCM varies and also to see how the melting front propagates and to capture the buoyancy effect as the battery is horizontally placed.

5.5 Contours of Melt fraction

Figure 21 shows the melt fraction/liquid fraction/volume fraction changes with respect to time. As per the collected data melting starts around t = 160 s when the heat generation inside the battery reaches equal to the melting point (T_m = 319 K) of the PCM. At first heat is transferred to the PCM by conduction mode and after the PCM is melt both conduction and convection heat transfer takes place at the mushy zone.

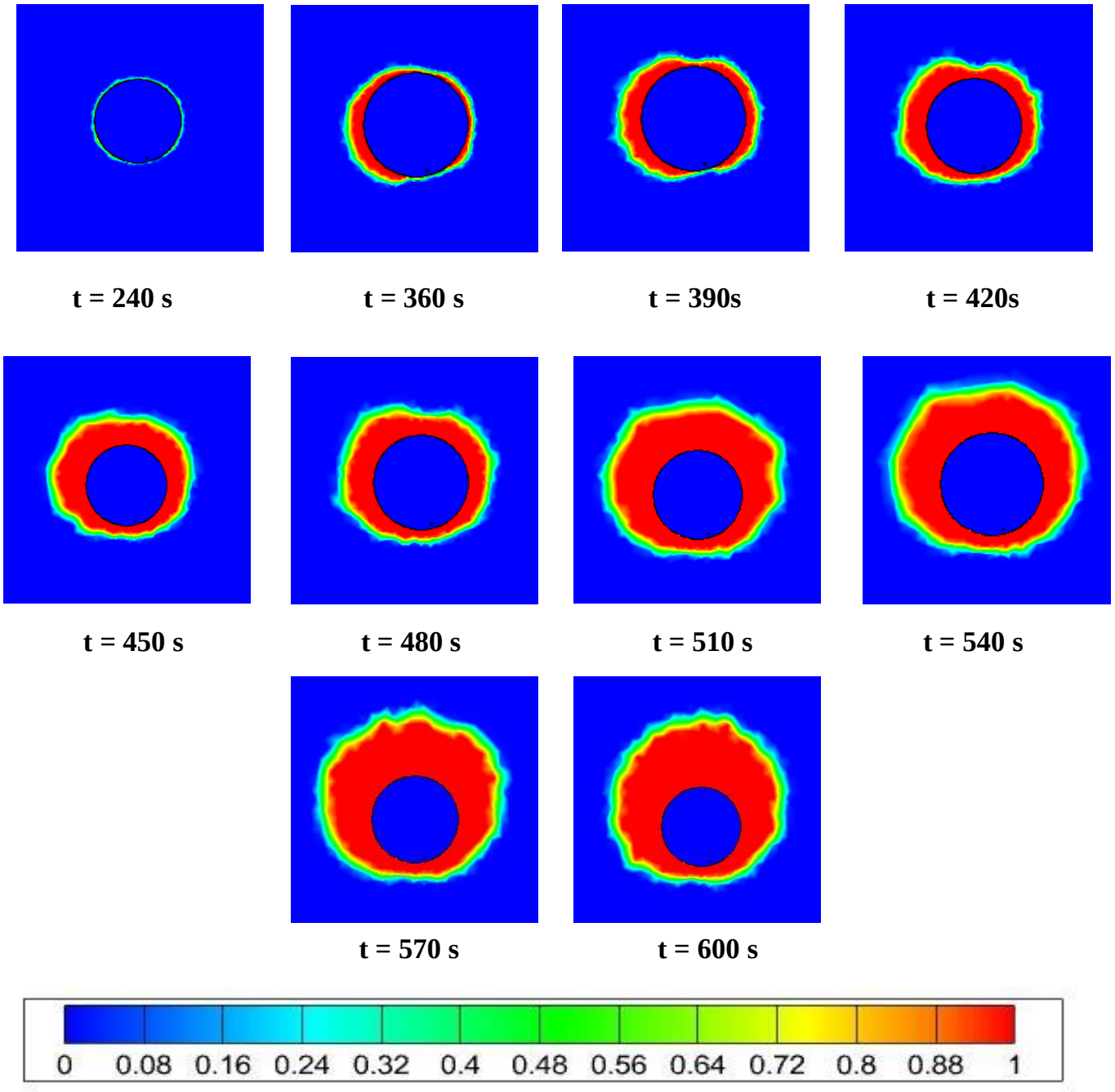

Figure 21: Melt fraction contours of PCM

We can observe that initially the melting starts from the periphery especially at the right and left side of the battery wall and less melting happens at the top of the battery. As time progresses and the PCM that is at the top of the battery melts, more and more melting occurs at that region. Due to melting the liquid PCM tends to melt more and more PCM that is above it due to buoyancy effect. That's why we can observe an upward movement of PCM melting. This can be observed after t = 450s.

5.6 Temperature Contours

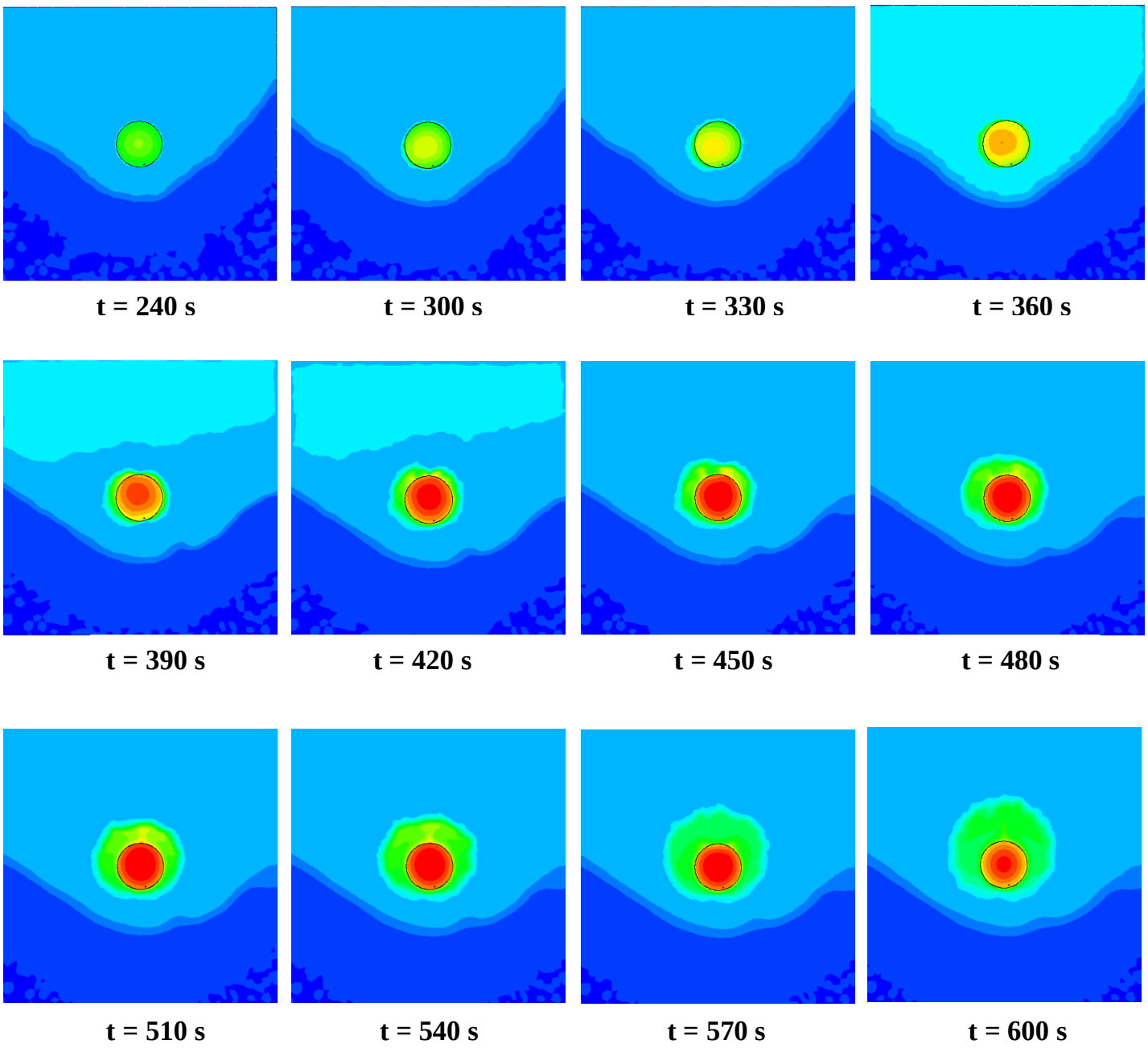

Figure 22: Temperature contours of battery and PCM during PCM cooling

Figure 22 describes the temperature contours of the battery and PCM zones during the PCM cooling. We can see as time progresses the heat generation in the battery increases due TR and the temperature inside the PCM zone also increases due to melting of the PCM. We can also see that only PCM is not able to withstand the high heat generation inside that battery due to poor conductivity that's why temperature inside the battery keeps on increasing. We can also observe that the upper zone (PCM) of the battery is more heated than the lower zone this is due to the same buoyancy effect.

5.7 Conclusions

From the comparison of air cooling and PCM cooling we can conclude that, for the given configuration of the battery PCM is better in comparison to the air which we have supplied but both are unable to keep the battery's temperature within the optimum level when used individually. We can see that PCM cannot save a battery from TR but it can surely save TR propagation from one battery to another. We can easily place the other battery packs at the edges of the square domain where the temperature is still 300 K. Also we have to use the various PCM performance enhancement techniques so that the PCM can conduct the heat faster and also we have to find an optimum level of PCM that needs to be used from a weight and cost perspective.

We have previously discussed that the heat generation rate that we have taken in this study is quite high so we can also perform this study using low C-rates in future studies to see how this cooling methods perform. We can also extend the study for multiple batteries to the effects of cooling and TR propagation from one battery to another.

References

1. Hatchard, T.D., MacNeil, D.D., Basu, A. and Dahn, J.R., 2001. Thermal model of cylindrical and prismatic lithium-ion cells. *Journal of The Electrochemical Society*, *148*(7), p.A755.

2. Kim, G.H., Pesaran, A. and Spotnitz, R., 2007. A three-dimensional thermal abuse model for lithium-ion cells. *Journal of power sources*, *170*(2), pp.476-489.

3. Coman, P.T., Mátéfi-Tempfli, S., Veje, C.T. and White, R.E., 2017. Modeling vaporization, gas generation and venting in Li-ion battery cells with a dimethyl carbonate electrolyte. *Journal of The Electrochemical Society*, *164*(9), p.A1858.

4. Panchal, S., Mathew, M., Fraser, R. and Fowler, M., 2018. Electrochemical thermal modeling and experimental measurements of 18650 cylindrical lithium-ion battery during discharge cycle for an EV. *Applied Thermal Engineering*, *135*, pp.123-132.

5. Coman, P.T., Darcy, E.C., Veje, C.T. and White, R.E., 2017. Modelling Li-ion cell thermal runaway triggered by an internal short circuit device using an efficiency factor and Arrhenius formulations. *Journal of The Electrochemical Society*, *164*(4), p.A587.

6. Lopez, C.F., Jeevarajan, J.A. and Mukherjee, P.P., 2015. Experimental analysis of thermal runaway and propagation in lithium-ion battery modules. *Journal of the electrochemical society*, *162*(9), p.A1905.

7. Cai, T., Stefanopoulou, A.G. and Siegel, J.B., 2019. Early detection for li-ion batteries thermal runaway based on gas sensing. *ECS Transactions*, *89*(1), p.85.

8. Feng, X., Ouyang, M., Liu, X., Lu, L., Xia, Y. and He, X., 2018. Thermal runaway mechanism of lithium ion battery for electric vehicles: A review. *Energy Storage Materials*, *10*, pp.246-267.

9. Wang, Q., Ping, P., Zhao, X., Chu, G., Sun, J. and Chen, C., 2012. Thermal runaway caused fire and explosion of lithium ion battery. *Journal of power sources*, *208*, pp.210-224.

10. Pesaran, A.A., 2001. Battery thermal management in EV and HEVs: issues and solutions. *Battery Man*, *43*(5), pp.34-49.

11. Tete, P.R., Gupta, M.M. and Joshi, S.S., 2021. Developments in battery thermal management systems for electric vehicles: A technical review. *Journal of Energy Storage*, *35*, p.102255.

12. Park, H., 2013. A design of air flow configuration for cooling lithium ion battery in hybrid electric vehicles. *Journal of power sources*, *239*, pp.30-36.

13. Cho, G.Y., Choi, J.W., Park, J.H. and Cha, S.W., 2014. Transient modeling and validation of lithium ion battery pack with air cooled thermal management system for electric vehicles. *International journal of automotive technology*, *15*(5), pp.795-803.

14. Lu, Z., Meng, X.Z., Wei, L.C., Hu, W.Y., Zhang, L.Y. and Jin, L.W., 2016. Thermal management of densely-packed EV battery with forced air cooling strategies. *Energy Procedia*, *88*, pp.682-688.

15. Chen, K., Wang, S., Song, M. and Chen, L., 2017. Configuration optimization of battery pack in parallel air-cooled battery thermal management system using an optimization strategy. *Applied Thermal Engineering*, *123*, pp.177-186.

16. Xie, J., Ge, Z., Zang, M. and Wang, S., 2017. Structural optimization of lithium-ion battery pack with forced air cooling system. *Applied Thermal Engineering*, *126*, pp.583-593.

17. Tong, W., Somasundaram, K., Birgersson, E., Mujumdar, A.S. and Yap, C., 2015. Numerical investigation of water cooling for a lithium-ion bipolar battery pack. *International Journal of Thermal Sciences*, *94*, pp.259-269.

18. Qian, Z., Li, Y. and Rao, Z., 2016. Thermal performance of lithium-ion battery thermal management system by using mini-channel cooling. *Energy Conversion and Management*, *126*, pp.622-631.

19. Li, K., Yan, J., Chen, H. and Wang, Q., 2018. Water cooling based strategy for lithium ion battery pack dynamic cycling for thermal management system. *Applied Thermal Engineering*, *132*, pp.575-585.

20. Chen, S., Peng, X., Bao, N. and Garg, A., 2019. A comprehensive analysis and optimization process for an integrated liquid cooling plate for a prismatic lithium-ion battery module. *Applied Thermal Engineering*, *156*, pp.324-339.

21. Liu, C., Xu, D., Weng, J., Zhou, S., Li, W., Wan, Y., Jiang, S., Zhou, D., Wang, J. and Huang, Q., 2020. Phase change materials application in battery thermal management system: a review. *Materials*, *13*(20), p.4622.

22. Al Hallaj, S. and Selman, J.R., 2000. A novel thermal management system for electric vehicle batteries using phase-change material. *Journal of the Electrochemical Society*, *147*(9), p.3231.

23. Khateeb, S.A., Farid, M.M., Selman, J.R. and Al-Hallaj, S., 2004. Design and simulation of a lithium-ion battery with a phase change material thermal management system for an electric scooter. *Journal of Power Sources*, *128*(2), pp.292-307.

24. Kizilel, R., Lateef, A., Sabbah, R., Farid, M.M., Selman, J.R. and Al-Hallaj, S., 2008. Passive control of temperature excursion and uniformity in high-energy Li-ion battery packs at high current and ambient temperature. *Journal of Power Sources*, *183*(1), pp.370-375.

25. Rao, Z., Wang, S. and Zhang, G., 2011. Simulation and experiment of thermal energy management with phase change material for ageing LiFePO4 power battery. *Energy Conversion and Management*, *52*(12), pp.3408-3414.

26. Javani, N., Dincer, I., Naterer, G.F. and Yilbas, B.S., 2014. Heat transfer and thermal management with PCMs in a Li-ion battery cell for electric vehicles. *International Journal of Heat and Mass Transfer*, *72*, pp.690-703.

27. Goli, P., Legedza, S., Dhar, A., Salgado, R., Renteria, J. and Balandin, A.A., 2014. Graphene-enhanced hybrid phase change materials for thermal management of Li-ion batteries. *Journal of Power Sources*, *248*, pp.37-43.

28. Greco, A., Jiang, X. and Cao, D., 2015. An investigation of lithium-ion battery thermal management using paraffin/porous-graphite-matrix composite. *Journal of Power Sources*, *278*, pp.50-68.

29. Rao, Z., Wang, S., Wu, M., Lin, Z. and Li, F., 2013. Experimental investigation on thermal management of electric vehicle battery with heat pipe. *Energy Conversion and Management*, *65*, pp.92-97.

30. Li, Y., Qi, F., Guo, H., Guo, Z., Xu, G. and Liu, J., 2019. Numerical investigation of thermal runaway propagation in a Li-ion battery module using the heat pipe cooling system. *Numerical Heat Transfer, Part A: Applications*, *75*(3), pp.183-199.

31. Qin, J., Zhao, S., Liu, X. and Liu, Y., 2020. Simulation study on thermal runaway suppression of 18650 lithium battery. *Energy Sources, Part A: Recovery, Utilization, and Environmental Effects*, pp.1-13.

32. Liu, T., Liu, Y., Wang, X., Kong, X. and Li, G., 2019. Cooling control of thermally-induced thermal runaway in 18,650 lithium ion battery with water mist. *Energy Conversion and Management*, *199*, p.111969.

33. Fadl, M. and Eames, P.C., 2019. Numerical investigation of the influence of mushy zone parameter Amush on heat transfer characteristics in vertically and horizontally oriented thermal energy storage systems. *Applied Thermal Engineering*, *151*, pp.90-99.

34. S.V. Patankar, Numerical Heat Transfer and Fluid Flow, Hemisphere, Washington DC, 1980.

35. Brent, A.D., Voller, V.R. and Reid, K.T.J., 1988. Enthalpy-porosity technique for modeling convection-diffusion phase change: application to the melting of a pure metal. *Numerical Heat Transfer, Part A Applications*, *13*(3), pp.297-318.

36. Brent, A.D., Voller, V.R. and Reid, K.T.J., 1988. Enthalpy-porosity technique for modeling convection-diffusion phase change: application to the melting of a pure metal. *Numerical Heat Transfer, Part A Applications*, *13*(3), pp.297-318.

37. Vogel, J.J.F.M.J., Felbinger, J. and Johnson, M., 2016. Natural convection in high temperature flat plate latent heat thermal energy storage systems. *Applied Energy*, *184*, pp.184-196.

38. M. Keyser, E. Darcy, D. Long, and A. Pesaran, Pat. No. US9142829 B2 (2015).

39. Kamkari, B., Shokouhmand, H. and Bruno, F., 2014. Experimental investigation of the effect of inclination angle on convection-driven melting of phase change material in a rectangular enclosure. *International Journal of Heat and Mass Transfer*, *72*, pp.186-200.